Structural Studies on Asparagine Synthetase
from *Escherichia coli* K-12

Toru Nakatsu

1997

Structural Studies on Asparagine Synthetase
from *Escherichia coli* K-12

Toru Nakatsu

1997

Contents

Abbreviations

aaRS	aminoacyl-tRNA synthetase
AMP	adenosine 5'-monophosphate
AS-A	asparagine synthetase [L-aspartate:ammonia ligase (AMP-forming) EC 6.3.1.1]
AS-B	asparagine synthetase [L-aspartate:L-glutamine amido-ligase (AMP-forming) EC 6.3.5.4]
AspRS	aspartyl-tRNA synthetase
ATP	adenosine 5'-triphosphate
B-factor	temperature factor
DEAE	diethylaminoethyl
DLS	dynamic light scattering
DTT	dithiothreitol
E. coli	*Escherichia coli*
EDTA	ethylenediaminetetraacetic acid
F_c	calculated structure factor
F_o	observed structure factor
GlnRS	glutaminyl-tRNA synthetase
HEPES	*N*-2-hydroxyethylpiperazine-*N'*-2-ethanesulfonic acid
IPTG	isopropyl β,D-thiogalactopyranoside
K_M	Michaelis constant
MIR	multiple isomorphous replacement
MIRAS	multiple isomorphous replacement with anomalous scattering
MW	molecular weight
PAGE	polyacrylamide gel electrophoresis
PEG	polyethylene glycol
R-factor	crystallographic residual value
R_H	hydrodynamic radius
R_{merge}	merging R-factor
S. cerevisiae	*Saccharomyces cerevisiae*
SDS	sodium dodecyl sulfate
SerRS	seryl-tRNA synthetase
Tris	tris (hydroxymethyl)aminomethane

CHAPTER 1

General Introduction

Asparagine synthetase [L-aspartate: ammonia ligase (AMP-forming) EC 6.3.1.1] (AS-A) catalyzes the synthesis of L-Asn from L-Asp and ammonia with the conversion of ATP into AMP and pyrophosphate in the presence of Mg^{2+} ion (Meister, 1974). AS-A is distributed in prokaryotes as *Escherichia coli* K-12 (Cedar *et al.*, 1969a) and *Klebsiella aerogenes* (Reitzer *et al.*, 1982) and encoded by *asnA* gene. The *asnA* gene from *E. coli* K-12 coded for a polypeptide of 330 amino acid residues with a molecular weight of 36700, and the AS-A exists such as a dimer of identical subunits (Nakamura *et al.*, 1981; Sugiyama *et al.*, 1992). In addition, the overexpression of the *asnA* gene and purification of AS-A have been established by Sugiyama *et al.*(1992).

The feature of the AS-A from *Escherichia coli* K-12 has been studied by Cedar *et al.* It is proposed that the catalytic reaction of AS-A is two-step mechanism involving intermediate formation of enzyme-bound β-aspartyl adenylate (Cedar *et al.*, 1969a), namely the first reaction step is the formation of enzyme-bound β-aspartyl adenylate intermediate from ATP and L-Asp, and the second step is the production of L-Asn by attacking ammonia to β-aspartyl adenylate intermediate (Figure 1-1). The existence of the aminoacyl-adenylate intermediate is supported by the following observations: AS-A catalyzes the transfer of oxygen from ^{18}O-labeled L-Asp to AMP, while no ^{18}O was found in the pyrophosphate; and the exchange reaction of pyrophosphate-ATP is dependent on the substrate L-Asp (Cedar *et al.*, 1969b). The formation of β-aspartyl adenylate intermediate is the rate-limiting step in the synthesis of L-Asn since the rate of the exchange of pyrophosphate-ATP is closely to
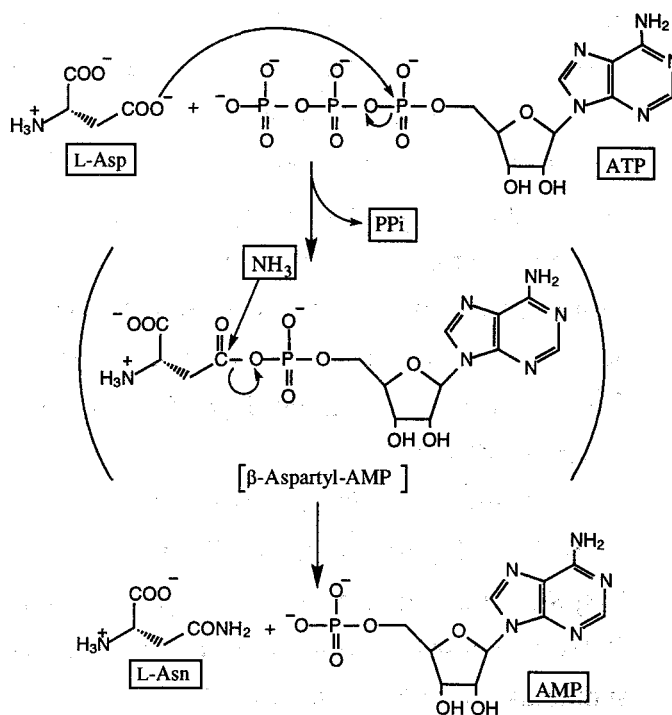

Figure 1-1. Reaction scheme of Asparagine Synthetase.

the over-all rate of L-Asn synthesis. Furthermore, it is proposed that the reaction mechanism of AS-A is the Bi Uni Uni Bi ping pong mechanism, that L-Asp and ATP add in a random order, and that L-Asn and AMP leave the enzyme in a random order (Cedar et al., 1969b). AS-A is essentially inactivate when ATP is replaced by ADP, UTP, CTP, and GTP (Cedar et al., 1969a). Magnesium ion is necessary for the synthesis of L-Asn and can not be replaced by manganese ion (Cedar et al., 1969a). Furthermore, glycerol and β-mercaptoethanol are stabilized AS-A, while sulfhydryl reagents such as p-hydroxymercuribenzoate, N-ethylmaleimide, and iodoacetamide is inactivated AS-A, indicating AS-A has reactive cysteine residues (Cedar et al., 1969a).

On the other hand, asparagine synthetase using L-Gln as amido nitrogen donor [L-aspartate: L-glutamine amido-ligase (AMP-forming) EC 6.3.5.4] (AS-B) is found not only in prokaryotes (Humbert et al., 1980; Reitzer et al., 1982) but also in eukaryotes (Gantt et al., 1981; Hongo et al., 1981; Luehr et al., 1985; Andrulis et al., 1987), and encoded by asnB gene. AS-B catalyzes the synthesis of L-Asn from L-Asp and L-Gln in the presence of ATP and Mg^{2+} ion (Meister, 1974) and forms enzyme-bound aspartyl-adenylate intermediate (Luehr et al., 1985). The reaction mechanism of AS-B is indicated to be the Uni Uni Bi Ter ping pong mechanism (Hongo et al., 1985). Thus, the reaction mechanism of AS-A of the ammonia-dependent enzymes is different from that of AS-B of the glutamine-dependent enzymes, although both enzymes form an enzyme bound aspartyl-adenylate intermediate. The asnB gene has been cloned and sequenced from E. coli (Scofield et al., 1990) as well as asnA gene. Furthermore the asnB gene from human has also been cloned and sequenced (Andrulis et al., 1987). A high degree of amino acid sequence similarity has been shown between the glutamine-dependent enzymes (AS-B from E. coli and the human), whereas no significant similarity has been found between the AS-A and the AS-B sequences nonetheless derived from the same origin, E. coli (Scofield et al., 1990). AS-B is a member of the purF family of glutamine-dependent amidotransferase on the basis of its primary structure (Zalkin, 1993).

Gatti et al.(1991) showed that the carboxyl-terminal region of AS-A had the short homologous motif (GGGIGxxR) of eukaryotic aspartyl-tRNA synthetase (AspRS), although AS-A is not significantly related to any sequence in the protein or DNA databases (Scofield et al., 1990). AspRS is a kind of aminoacyl-tRNA synthetases (aaRSs), which are key enzymes in protein biosynthesis. The aaRSs have the two step reaction mechanism in analogy with AS-A: the first step is the formation of an enzyme-bound aminoacyl-adenylate intermediate in which the amino acid is activated by phosphorylation to the α-phosphate of AMP, and the second step is the

transfer of the amino acid moiety to either the 2'-hydroxyl or 3'-hydroxyl group of the terminal ribose of the cognate tRNA (Schimmel, 1987). The aaRSs are classified by the primary site of phosphorylation of the amino acid to the hydroxyl group of the tRNA terminal ribose: class I (LeuRS, IleRS, ValRS, CysRS, MetRS, TyrRS, TrpRS, GluRS, GlnRS, ArgRS) enzymes are the 2'-hydroxyl group and class II (SerRS, ThrRS, ProRS, HisRS, AspRS, AsnRS, LysRS, GlyRS, AlaRS, PheRS) enzymes are the 3'-hydroxyl group except for PheRS (Eriani et al., 1990). The three dimensional structures of the both enzymes are determined, thereby the crystal structures of the catalytic domain are also classified: class I has the nucleotide binding (Rossmann) fold, while class II has antiparallel β-sheet flanked with two long α-helices (Moras, 1992; Cusack, 1995).

In the light of enzymatic mechanism that both AS-A and AspRS have common substrates; ATP and L-Asp, it has been proposed that the homologous region (GGGIGxxR) is participated in the binding of L-Asp or in the catalytic mechanism necessary to form an aspartyl-adenylate intermediate (Gatti et al., 1991; Hinchman et al., 1992). Hinchman et al.(1992) have found that Arg299 of AS-A in the motif (^{292}GGGIGxxR^{299}), which aligns with an invariant arginine residue in all reported classII aminoacyl-tRNA synthetases, directly participates a functional importance in the asparagine synthetase activity using site-directed mutagenesis. However, precise knowledge for the catalytic residues in particular for structure-function relationship is not available.

In this study, the author has aimed to understand the structural basis for the catalytic functions of AS-A by X-ray crystallography. In Chapter 2, the author has crystallized the E. coli AS-A and studied its preliminary X-ray crystallographic analysis. In Chapter 3, the author has determined the three dimensional structure of a binary complex with L-Asn (AS-A:L-Asn complex) at 2.5 Å resolution by the method of multiple isomorphous replacement (MIR). The structure has allowed to discuss its evolutional aspects related with the catalytic function. In Chapter 4, the author has also determined the three dimensional structure of a ternary complex with AMP and L-Asn (AS-A:AMP:L-Asn complex) at 2.2 Å resolution. Based on the structure, the author has implicated catalytically important residues and their roles in the enzymatic reaction.

CHAPTER 2

Crystallization of Asparagine Synthetase

2 - 1. Introduction

In order to get the single crystals suitable for X-ray crystallography, the protein must be not only pure but also homogeneous in terms of conformation and molecular distribution (Lorber *et al.*, 1992). Recently dynamic light scattering (DLS) is used for the investigation of the homogeneity of the protein before screening the crystallization conditions. The degree of homogeneity or the molecular distribution of the protein is given by the distribution of the hydrodynamic radius (R_H) in DLS analysis. The distribution of R_H of a homogeneous protein solution gives a narrow peak, while a heterogeneous protein solution shows a broad distribution of R_H. Namely the distribution of R_H thus correlates well with the degree of homogeneity of the protein under a given condition and the behavior of the protein. Ferré-D'Amaré *et al*, (1994a) monitored the behavior of the mutants of upstream stimulatory factor (USF) by using DLS and successfully crystallized the USF mutant. Since the DLS analysis of the native USF showed a very broad distribution of R_H, indicating that the USF was heterogeneous. They prepared several USF mutants by site-directed mutagenesis to improve the homogeneity of the USF. The DLS analysis of the mutants by DLS indicated a USF mutant, in which both amino- and carboxy-terminal residues were truncated, gave the narrowest distribution among the mutants prepared. This mutant readily crystallized, and the crystal structure was successfully determined Ferré-D'Amoré *et al.*, (1994b).

The author started the screening of the crystallization conditions of AS-A in order to determine the three dimensional structure by X-ray crystallography. For this purpose, a large quantity of highly purified AS-A was needed. The overexpression and the purification of AS-A were already reported by Sugiyama *et, al.* (1992), but the purity was insufficient to make good crystals suitable for X-ray diffraction analysis. The author therefore started the study by improving the purification method of AS-A prior to the screening of the crystallization conditions. As the results, the purification successfully improved by adding the previous method to the hydrophobic chromatography and gave the highly purified AS-A. The crystallization of the wild type AS-A, however, gave only needles unsuitable for X-ray diffraction analysis. This seemed to have caused by the oxidation of AS-A during the crystallization because

4

preliminary analysis by polyacrylamide gel electrophoresis (PAGE) indicated that the wild type AS-A produced several oligomeric forms under oxidative conditions by compulsion. It was presumed that the cysteine residues of AS-A were responsible for the oxidative oligomerization. The author thus decided to replace the suspected cysteine residues with alanine by site directed mutagenesis to prevent the unwanted oxidative oligomerization. The heterogeneity of the wild type AS-A by oligomerization was also confirmed by DLS, a technique for measuring. DLS analysis of the mutant enzyme showed that the mutant was structurally homogeneous and suitable for the crystallization compared to the wild type. Thus the author succeeded in getting the single crystals suitable for X-ray crystallography by using the mutant AS-A.

In this chapter, an improved purification of the AS-A is described first and secondary, mutant AS-As are prepared and their behavior is characterized by PAGE and DLS, and finally the crystallographic study of the Cys-free mutant is described.

2 - 2. Experimental Procedures

Materials

Plasmid pUNAd37 is a pUC18 derivative containing *asnA* gene (Nakamura *et al.*, 1981; Sugiyama *et al.*, 1992). *E.coli* JM109 was provided by Takara Shuzo Co., Ltd. (Kyoto, Japan). DEAE-Cellulofine A-800m and Blue-Cellulofine were gifts from Chisso Co. (Minamata, Japan). Phenyl-TOYOPEARL 650 was obtained from TOSOH Co., Ltd. (Tokyo, Japan). Ammonium sulfate (specially prepared reagent: code No. 026-20) for crystallization was purchased from Nacalai Tesque Inc. (Kyoto, Japan). CYSCHEM MVD/24 plate and glass capillaries were obtained from Charles Supper Company.

Overexpression and Purification of AS-A

E. coli JM109 transformed with the plasmid pUNAd37 was grown at 37 °C with reciprocal shaking in 3 L of LB medium (1% bacto-tryptone, 0.5 % bacto-yeast extract, 1% NaCl, pH7.5) supplemented with 50 mg/mL ampicillin. Isopropyl-β-D-thiogalactopyranoside was added to a final concentration of 1 mM at the log phase (OD_{600} was about 0.7). After 14 hours, the cells were harvested by centrifugation at 8000 × g for 5 minutes, and suspended in 100 mL of buffer A [20 mM Tris-HCl (pH 7.8), 10 mM Mg(OAc)$_2$, 1mM EDTA, 30 mM KCl, and 5 mM β-mercaptoethanol] and collected again by centrifugation. The cells were then suspended in 100 mL of buffer A and disrupted by sonication at 0 °C. The mixture was centrifuged at 25000 × g for 20 minutes to remove cellular debris. The resulting cell-free extract was diluted to about 5

mg/mL of protein concentration with buffer B [20 mM Tris-HCl (pH7.4) containing 10 % (w/v) glycerol, and 5 mM β-mercaptoethanol], and applied to a DEAE-Cellulofine A-800m column (5 cm $\phi \times$ 20 cm) equilibrated with the same buffer. After the column was washed with 1 L of the buffer B containing 0.12 M KCl, elution was done with a linear gradient from 0.12 M to 0.4 M KCl in buffer B. The active fraction, eluted at a KCl concentration of approximately 0.25 M, was concentrated to about 10 mL with a membrane Type YM-10 (Amicon Co.). The concentrated solution was dialyzed against buffer B containing 10 mM Mg(OAc)$_2$ and was applied to a Blue-Cellulofine column (2.6 cm $\phi \times$ 19 cm) equilibrated with the same buffer. The column was washed with buffer B containing 10 mM Mg(OAc)$_2$ and 0.1 M KCl, and was then eluted with a linear gradient from 0.1 M KCl and 10 mM Mg(OAc)$_2$ to 1.0 M KCl and 0 mM Mg(OAc)$_2$ in buffer B (Sugiyama et al., 1992). To the active fraction was added powdered ammonium sulfate with gentle stirring to 20 % saturation at 0 °C. The solution was applied to a Phenyl-TOYOPEARL 650 column (2.6 cm $\phi \times$ 19 cm) equilibrated with 0.8 M ammonium sulfate in buffer B. After the column was washed with 200 mL of the same buffer, elution was carried out with a linear gradient from 0.8 to 0 M ammonium sulfate in buffer B. The enzyme was eluted at an ammonium sulfate concentration of approximately 0.5 M. The active fraction was dialyzed against buffer C [20 mM HEPES (pH 7.5) containing 10 % (w/v) glycerol, and 5 mM β-mercaptoethanol] and was concentrated to 30 mg/mL by using a membrane Type YM-10 (Amicon Co.). The purity was judged by SDS-PAGE (Laemmli, 1970), and the protein solution was store at -20 °C.

Measurement of AS-A Activity

The concentration of protein was measured by Protein Assay Reagent (Pierce Chemical Co.), with bovine serum albumin was used as a standard. The protein concentration of the purified AS-A preparation was determined spectrophotometrically at 280 nm, using an extinction coefficient of $A_{280}^{1\%}$ = 13.9 cm^{-1}. The activity of AS-A was assayed spectrophotometrically by measuring AMP formation with an adenylate kinase-pyruvate kinase-lactate dehydrogenase coupled enzyme assay. A solution of AS-A (50 µl) was added to an assay medium containing 2 U adenylate kinase, 10 U pyruvate kinase, 25 U lactate dehydrogenase, 0.24 mM NADH, 1 mM phosphoenolpyruvate, 1.5 mM L-aspartic acid, 20 mM NH$_4$Cl, 3 mM ATP, 100 mM KCl, 10 mM Mg(OAc)$_2$, and 5 mM β-mercaptoethanol in Tris-HCl buffer (pH7.8) of a total volume of 1 mL, and the decrease of NADH was monitored at 340 nm. One unit of enzyme was defined as the

amount of enzyme that catalyzed the formation of 1 μmol of asparagine per minute at 37 °C (Sugiyama *et al.*, 1992).

Crystallization

The purified 10 mg/mL AS-A protein solution including 2 mM HEPES (pH7.5) containing 10 % glycerol and 5 mM β-mercaptoethanol was used for the screening of the crystallization conditions of AS-A. The crystallization was carried out by using a hanging drop or a sitting drop vapour diffusion method. The screening was carried out by changing the conditions such as precipitant, buffer, pH, additive and temperature. The reservoir solution (1 mL) was prepared by mixing an appropriate precipitant and additives in a buffer with various pHs and was mixed with the solution of AS-A to make a drop. Each drop consisted of 2 μl of the protein solution and 2 μl of the reservoir solution. The reagents and temperatures used for the screening were:

Precipitant: ammonium sulfate; lithium sulfate; lithium chloride; sodium chloride; potassium sodium tartrate; polyethylene glycol (PEG) 400; PEG1000; PEG4000; PEG6000; PEG8000; 2-methyl-2,4-pentanediol.

Buffer: MES (pH6.5); MOPS (pH7.0 and 7.5); HEPES (pH7.5); Tris-HCl (pH7.5 and 8.0); TAPS (pH8.5).

Additive: ATP; AMP; L-Asp; L-Asn; $MgCl_2$; β-octylglucoside; dimethyl sulfoxide.
Temperature: 4 °C; 20 °C.

Oxidation and Reduction of AS-A

The reduced form of AS-A was prepared by adding 20 mM DTT in buffer I [20 mM Tris-HCl (pH7.4), 10 % glycerol, 0.1 mM EDTA] including 20 mM DTT to the purified AS-A followed by incubation for one hour. The DTT was then removed by gel filtration on sephadex G-25, and the solution was concentrated by using Centricon (Amicon Co.). The concentration of the reduced AS-A was adjusted to 4 mg/mL by dilution with buffer I. The reduced form of AS-A was analyzed with polyacrylamide gel electrophoresis under the reductive conditions.

The oxidized form of AS-A was prepared by the following procedure: 5 mM $K_3Fe(CN)_6$ (5 μl) was added to the 4 mg/mL reduced form AS-A (45 μl). The mixture was incubated at 4 °C for 48 hours. The oxidized form of AS-A was analyzed with polyacrylamide gel electrophoresis under the non-reductive conditions.

Polyacrylamide Gel Electrophoresis

AS-A was analyzed by 10 % SDS-PAGE and 7.5 % Native-PAGE according to the

methods of Laemmli (Laemmli, 1970) and Davis (Davis, 1964), respectively. The SDS-PAGE and the Native-PAGE were carried out at room temperature and 4 °C, respectively.

Site Directed Mutagenesis

The AS-A mutants C51A (Cys51→Ala), C315A (Cys315→Ala) and Cys-free (Cys51→Ala and Cys315→Ala) of AS-A were produced by Kunkel's method (Kunkel, 1985; Kunkel *et al.*, 1987). The mutagenic oligonucleotide primers were 5'-CTTGTCGGGCGCTGAAAAAGCG-3' (Cys51→Ala), and 5'-CCAGGTTCAGGCCGGCGTATGGCCAGC-3' (Cys315→Ala). The resulting DNA sequence was confirmed by dideoxy sequencing (Sanger *et al.*, 1977). The mutant gene was subcloned into an expression plasmid pUNAd37 (Sugiyama *et al.*, 1992).

Dynamic Light Scattering

A purified protein solution (1 mg/mL) in 2 mM HEPES (pH 7.5) containing 1 % glycerol and 5 mM β-mercaptoethanol was prepared. The solution (300 μl) was filtered through Anatop10 membrane with the pore size of 0.02 μm or 0.1 μm (Whattman Inc.) and was injected manually into the sample cell of the DynaPro-801 (Protein Solutions Inc., USA). The measurement was continually carried out at room temperature to collect 25 points of data over five minutes.

Precession Photographs of Cys-free AS-A Crystals

A crystal of the Cys-free AS-A in a thin-walled glass capillary was mounted on a precession photograph, model FR504 (Enraf-Nonius Inc.). Precession photographs were taken with Ni-filtered Cu $K\alpha$ radiation from an RU-200 rotating anode (Rigaku Co., Ltd., Tokyo, Japan) operated at 40 kV and 100 mA. The conditions for the data collection of the precession photographs were: crystal-to-detector distance, 100 mm; precession angle, 15 degrees; exposure time, 22 hours.

X-ray Diffraction Data Collection and Reduction of Cys-free AS-A Crystals

The X-ray diffraction intensity data of the crystals of Cys-free AS-A were collected on an R-AXIS IIc imaging plate area detector (Rigaku, Tokyo, Japan) with monochromatized Cu $K\alpha$ radiation from an RU-300 rotating anode (Rigaku, Tokyo, Japan) operated at 40 kV and 100 mA. The data were reduced by using an R-AXIS IIc software (Sato *et al.*, 1992). Self-rotation functions were calculated for polar angle by

using the program POLARRFN of the CCP4 suit (Collaborative computational project, 1994).

2 - 3. Results and Discussion

Improvement of Purification

Sugiyama et. al., (1992) reported that AS-A could be purified by DEAE-Cellulofine A-800m and Blue-Cellulofine , but the author found that the purified AS-A by this procedure contained a trace of impurities. Thus the SDS-PAGE of the purified enzyme showed an extra band except for AS-A at the position corresponding to the molecular weight (MW) of about 90000. The purity of the sample was insufficient for crystallization, and the AS-A had to be further purified. After trials of several types of chromatography, contaminating protein was successfully removed by a hydrophobic chromatography using Phenyl-TOYOPEARL 650. The chromatography on Phenyl-TOYOPEARL 650 resulted in a total of 1.1-fold increase in the purity of AS-A. The final protein sample should not contain impurities since a highly purified AS-A was required to obtain the crystals suitable for X-ray diffraction analysis. The results of the purification are summarized in Table 2-1.

Table 2-1. Purification of Asparagine Synthetase.

	Total protein (mg)	Specific activity (unit[§] / mg)	Total activity (unit[§])	Recovery (%)	Purity (-fold)
Crude extract	1290	3.2	4128	100	1.0
DEAE-Cellulofine A-800m	310	12.7	3922	95.0	4.0
Blue-Cellulofine	78	21.4	1669	40.4	6.7
Phenyl-TOYOPEARL 650	50	22.4	1120	27.1	7.0

[§]One unit of enzyme was defined as the amount of enzyme producing 1 μmole of L-Asn per min. under the assay conditions.

Characterization of Wild Type AS-A

In the first place, the crystallization of the wild type AS-A was tried under several crystallization conditions. The crystals of the wild type AS-A were obtained by using ammonium sulfate as precipitant in a week at 20 °C. However, the crystals obtained were fine needles of 0.3 mm of length and 0.02 mm of width (Figure 2-1) and were not suitable for X-ray diffraction analysis, because the size of the crystals was too small.

The crystallization conditions were improved by changing the conditions such as the buffers, pH and additives (substrate or detergent). However, the quality of the crystals was not improved. The failure seemed to have caused by the oxidation of AS-A because Cedar *et al.,* (1969a) reported that AS-A was stabilized by adding the reductant such as β-mercaptoethanol. Actually, AS-A is inactivated without β-mercaptoethanol and by the sulfhydryl such as *p*-hydroxymercuribenzoate, *N*-ethylmaleimide, and iodoacetamide. Hence the behavior of the wild type AS-A was examined under oxidative and reductive conditions to prove the reason for the failure in crystallization.

Figure 2-1. Crystal of wild type Asparagine Synthetase.

The wild type AS-A was oxidized with Fe^{3+} and was analyzed with SDS-PAGE under the non-reductive conditions. As shown in Figure 2-2, the SDS-PAGE gave three bands, which corresponded to the calculated MW of about 38000, 75000, and 100000. The band at the MW of 38000 corresponded to the subunit of AS-A (MW 36700), and the bands at the MW of 75000 and 100000 were likely to correspond to the dimer (MW 73400) and the trimer (MW 110100) of AS-A, respectively. It seems therefore that the oxidized form of the wild type AS-A has at least three different types of molecules. On the other hand, the wild type AS-A reduced by DTT was analyzed by SDS-PAGE under the reductive conditions. The SDS-PAGE showed only a single band of the MW of 38000. Thus the additional two molecular species observed for the oxidized AS-A appeared to have been produced by the oxidative formation of
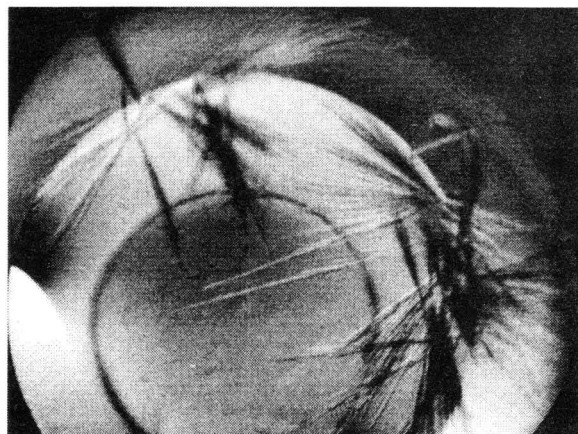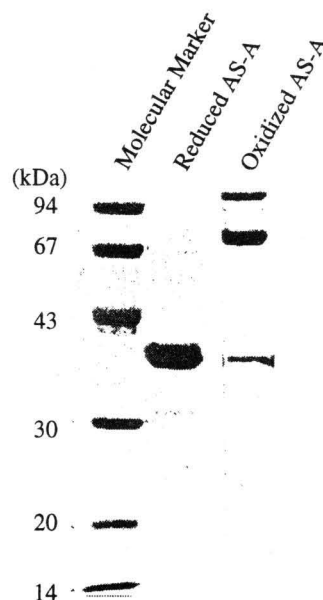

Figure 2-2. SDS-PAGE of the reduced and oxidized form of wild type Asparagine Synthetase.

the intersubunit disulfide linkage. The subunit of AS-A contains two cysteine residues (Cys51 and Cys315) (Nakamura *et al.*, 1981). The author assumed that at least one cysteine residue was responsible for the disulfide linkage. Hence 5 mM β-mercaptoethanol was added to the solution for the crystallization, but the quality of the crystals of the wild type AS-A was not improved. This suggested that the wild type AS-A is highly prone to form the intersubunit disulfide linkage spontaneously even in the presence of the reducing agent. The author therefore concluded that the wild type AS-A is unsuitable for the crystallization and that the cysteine residue of the wild type AS-A must be replaced with alanine by site directed mutagenesis so that the AS-A could not form the intersubunit disulfide linkage. It was anticipated that the mutant is adequate for the crystallization.

Site Directed Mutagenesis of AS-A

It was found that the wild type AS-A easily forms oligomers by the intersubunit disulfide linkage. It was assumed that Cys51 and Cys315 are responsible for the oligomerization. Thus the site directed mutagenesis of these cysteine residues was performed in order to prevent the oxidation of AS-A. Three types of Cys→Ala mutant of AS-A were prepared: C51A (Cys51→Ala), C315A (Cys315→Ala), and Cys-free (Cys51→Ala and Cys315→Ala). The plasmids carrying the mutant genes, C51A, C315A and Cys-free, are designated as pUNAd37C51A, pUNAd37C315A, and pUNAd37Cys-free, respectively. Since the behavior of these mutants with regards to the overexpression and purification were the same as the wild type AS-A, these mutants were successfully prepared by the same way as that of the wild type AS-A. The specific activity of C51A was almost identical with the wild type, and the C315A and Cys-free mutants were as about 33 % active as that of the wild type. Table 2-2 summarizes the specific activity of the wild type and the three mutants.

Table 2-2. Specific activity of wild type and mutants Asparagine Synthetase.

	Specific activity (unit[§] / mg)	Relative activity (%)
Wild	22.0	100
C51A	22.4	102
C315A	8.0	36
Cys-free	7.2	33

[§]One unit of enzyme was defined as the amount of enzyme producing 1 μmole of L-Asn per min. under the assay conditions.

Characterization of Mutant AS-As

The wild type AS-A consisted of at least three different molecular species under the oxidation conditions (Figure 2-2). Three types of Cys → Ala mutants were produced so as to improve the oxide-reductive character of the wild type. Thus the mutants were analyzed with the SDS-PAGE and Native-PAGE to see if their native was actually improved.

As shown in Figure 2-3, the SDS-PAGE of the reduced form of the three mutants gave a single band corresponding to the MW of 38000 as observed for the wild type under the reductive conditions. The oxidized form of the C315A mutant showed two bands in the SDS-PAGE, which corresponded to the MW of 38000 and 70000. Thus the C315A mutant also seems to produce the oligomer as observed for the wild type. On the other hand, the oxidized form of the C51A and Cys-free mutants gave the only one band at the MW of 38000 in the SDS-PAGE, indicating that the C51A and Cys-free mutants did not form the oligomers by the oxidation. It was therefore concluded that the Cys51 is responsible for the intersubunit disulfide formation. The C315A mutant is thus unsuitable for the crystallization as the wild type AS-A.

The wild type and mutants AS-A were then analyzed with Native-PAGE to investigate the properties under the native conditions without SDS. As shown in Figure 2-4, the reduced form of the wild type and C51A mutant gave two broad bands, suggesting that these enzymes consist of two different molecular species. Thus the C51A, which was judged as suitable for crystallization by the result of SDS-PAGE, seems to be unsuitable for the crystallization as judged by the Native-PAGE. On the other hand, the reduced form of the C315A and Cys-free mutants showed only one band in the Native-PAGE. The C315A and Cys-free mutants are likely to consist of a homogeneous conformer. Interestingly, all of the oxidized form of the wild type and three mutants gave a single band in the Native-PAGE, indicating that the oxidized enzymes consist of a single form of molecules under the conditions of the Native-PAGE, although the SDS-PAGE of the wild type and the C315A gave three bands.

The results of the characterization of the wild type and the three mutants of AS-A are summarized below. The wild type and the C315A mutant easily form the oligomers spontaneously under the oxidative conditions, and the wild type and the C51A mutant are heterogeneous under the reductive conditions. Therefore the wild type, the C51A, and the C315A are not suitable for the crystallization. Of all the three mutants, only the Cys-free mutant keeps homogeneity under both the reductive and oxidative conditions. Consequently the Cys-free mutant seems to be suitable for the crystallization.
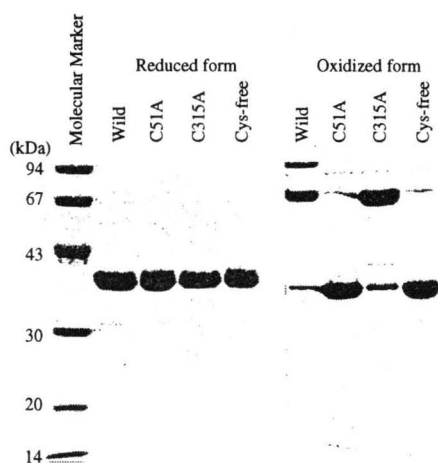
Figure 2-3. SDS-PAGE of the reduced form and the oxidized form Asparagine Synthetases (Wild, C51A, C315A, and Cys-free).

Figure 2-4. Native-PAGE of the reduced form and the oxidized form Asparagine Synthetases (Wild, C51A, C315A, and Cys-free).

Crystallization of Cys-free AS-A

It was found that the Cys-free mutant AS-A appears to be suitable for the crystallization as judged by the analysis with the SDS- and Native-PAGE. Before the screening of the crystallization conditions of the Cys-free, the homogeneity of the Cys-free AS-A was analyzed with dynamic light scattering (DLS) under the reductive conditions in order to investigate the behavior of the Cys-free mutant as compared to that of the
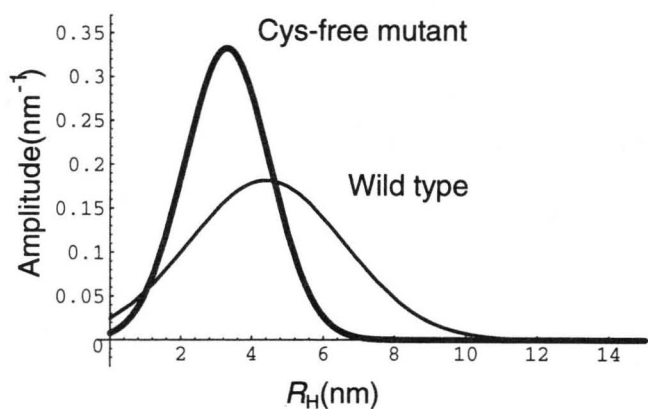
Figure 2-5. Distribution of hydrodynamic radius (R_H) determined by dynamic light scattering for wild type and Cys-free Asparagine Synthetase. The measurements were performed using a DynaPro-801. Thick line shows Cys-free Asparagine Synthetase, and thin line shows wild type Asparagine Synthetase.

wild type AS-A. Figure 2-5 shows the distribution of the hydrodynamic radius of the Cys-free and the wild type AS-A determined by DLS. The Cys-free mutant gave a narrow distribution with a standard deviation of 1.2 Å, while the wild type showed a broad distribution with a standard deviation of 2.2 Å, suggesting that the degree of homogeneity of AS-A was improved by replacing the cysteine residues (Cys51 and Cys315) with alanine by site directed mutagenesis. The narrower molecular distribution

13

of the Cys-free mutant is consistent with that of the analysis with the PAGEs. The Cys-free mutant is homogeneous, while the wild type AS-A is heterogeneous. This indicates that the chances of getting the crystals of AS-A suitable for X-ray diffraction analysis is also increased. The crystallization was then started with the Cys-free AS-A.

The author screened the crystallization conditions of the Cys-free AS-A by changing such as precipitant, buffer, pH, and additive. The Cys-free AS-A successfully crystallized in plates. Figure 2-6 shows the crystal of the Cys-free AS-A. The crystals were obtained by the sitting drop vapour diffusion method at 20 °C using a reservoir solution of 45 % saturated ammonium sulfate, 50 mM HEPES (pH 7.5), 22 mM L-Asn, 88 mM $MgCl_2$, 10 % (w/v)
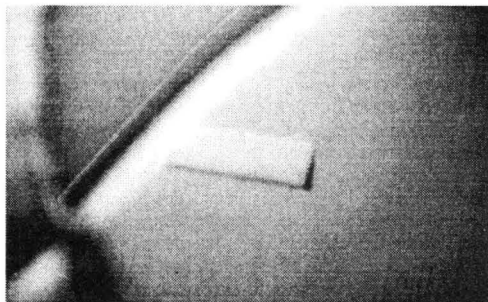
Figure 2-6. Crystal of Cys-free Asparagine Synthetase.

glycerol, and 5 mM β-mercaptoethanol. The drop contained equal volumes of the reservoir solution and the solution of 30 mg/mL AS-A including 20 mM HEPES (pH7.5), 10 % (w/v) glycerol and 5 mM β-mercaptoethanol. The crystals reached to a maximum size of 0.5 mm × 0.3 mm × 0.07 mm within three weeks. The crystallization conditions of the Cys-free AS-A are summarized in Figure 2-7. The absence of L-Asn from the crystallization conditions resulted in formation of twin crystals, which the plate crystals were stacked. Addition of the other ligands (ATP, AMP and L-Asp) for AS-A did not produce any good single crystals.

Drop solution (4μl)		
15	mg / ml	AS-A
23	% sat.	$(NH_4)_2SO_4$
35	mM	HEPES (pH7.5)
10	% (w/v)	Glycerol
5	mM	β-mercaptoethanol
11	mM	L-Asn
44	mM	$MgCl_2$

Reservoir solution (1ml)		
45	% sat.	$(NH_4)_2SO_4$
50	mM	HEPES (pH7.5)
10	% (w/v)	Glycerol
5	mM	β-mercaptorethanol
22	mM	L-Asn
88	mM	$MgCl_2$
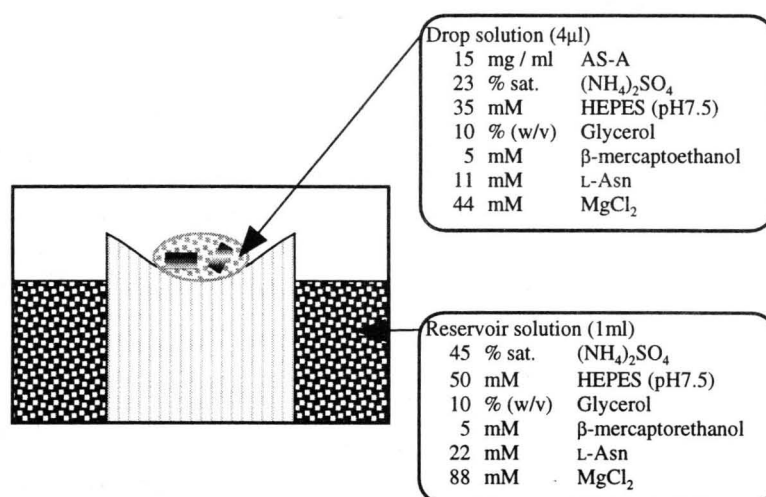
Figure 2-7. Crystallization of Cys-free Asparagine Synthetase by the sitting drop vapour diffusion method.

Crystallographic Data of Cys-free AS-A Crystals

The precession photographs of the crystals of the Cys-free AS-A indicated that the crystal system of the crystals was monoclinic. Figure 2-8 shows the precession photograph with respect to the $(h\,k\,0)$ plane of the crystal. The space group of $P2_1$ were specified by the extinction rule of reflection k = 2n + 1. The unit cell dimensions of the crystals were determined as a = 53 Å, b = 126 Å, c = 53 Å, and β = 105.5 ° from the precession photographs. The X-ray diffraction intensity data to a resolution of 2.5 Å [I > 1σ (I)] were collected on an R-AXIS IIc imaging plate with an R_{merge} of 10.5 %. The unit cell parameters were refined to a = 52.9 Å, b = 126.2 Å, c = 52.8 Å, β= 105.3 ° by the autoindexing routine of an R-AXIS IIc processing software. Summary of the crystallographic parameters and the data collection are shown in Table 2-3 and 2-4, respectively. Assuming that one dimer is in the asymmetric unit, a solvent content and a V_M were 47 % and 2.3 Å³/Da, respectively. The value of solvent content was within the normal range (27 - 65 %) for protein crystals (Matthews, 1968).

The self-rotation function gave significant peaks related to only two-fold rotation axis (κ = 180°) oriented with polar angles (ϕ = 90.5°, ψ = 166.1°) as shown in Figure 2-9. Using data from 10.0 Å to 3.5 Å, the peaks on the κ = 180° section were 55% that of the origin peak. The peak indicated that the two subunits of the homodimer are related with respect to a non-crystallographic two-fold rotation axis.
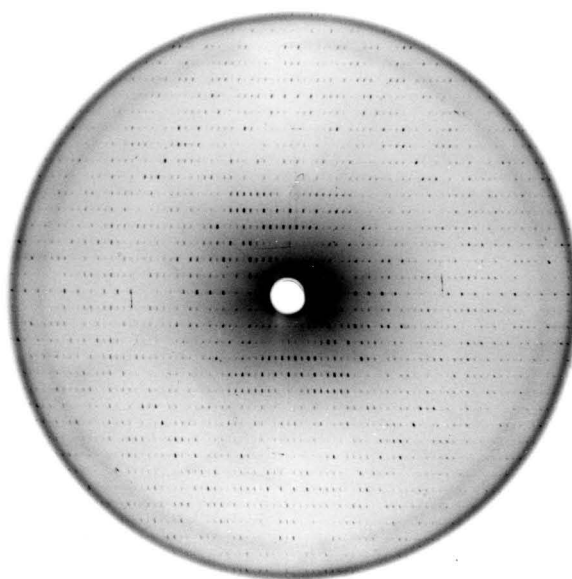
Figure 2-8. Precession Photograph $(h\,k\,0)$ plane of the Cys-free Asparagine Synthetase crystal.

Table 2-3. Crystallographic parameters of the Cys-free Asparagine Synthetase crystal.

Crystal system	:	monoclinic
Space group	:	$P\,2_1$
a	=	52.9 Å
b	=	126.2 Å
c	=	52.8 Å
β	=	105.3 °
Z	=	4 subunits
V_M	=	2.32 Å^3 Da^{-1}
V_{solv}	=	47 %

Table 2-4. Summary of data collection of Cys-free Asparagine Synthetase crystal.

Camera length (mm)	100.0
Spindle axis	-a*
Oscillation angle (degree / frame)	1.5
Exposing time (min. / frame)	20
No. of photos	92
Resolution (Å)	2.5
R_{merge} (%)[1]	10.45
Accepted reflections ($I > 1\sigma\,(I)$)	50944
Unique reflections ($I > 1\sigma\,(I)$)	17805
Completeness (∞ - 2.5 Å) (%)	73.8
Completeness (2.6 - 2.5 Å) (%)	54.5
Temperature (°C)	20

$$R_{merge} = \frac{\sum\sum\left|\langle I_{h,i}\rangle - I_{h,i}\right|}{\sum\sum I_{h,i}}$$
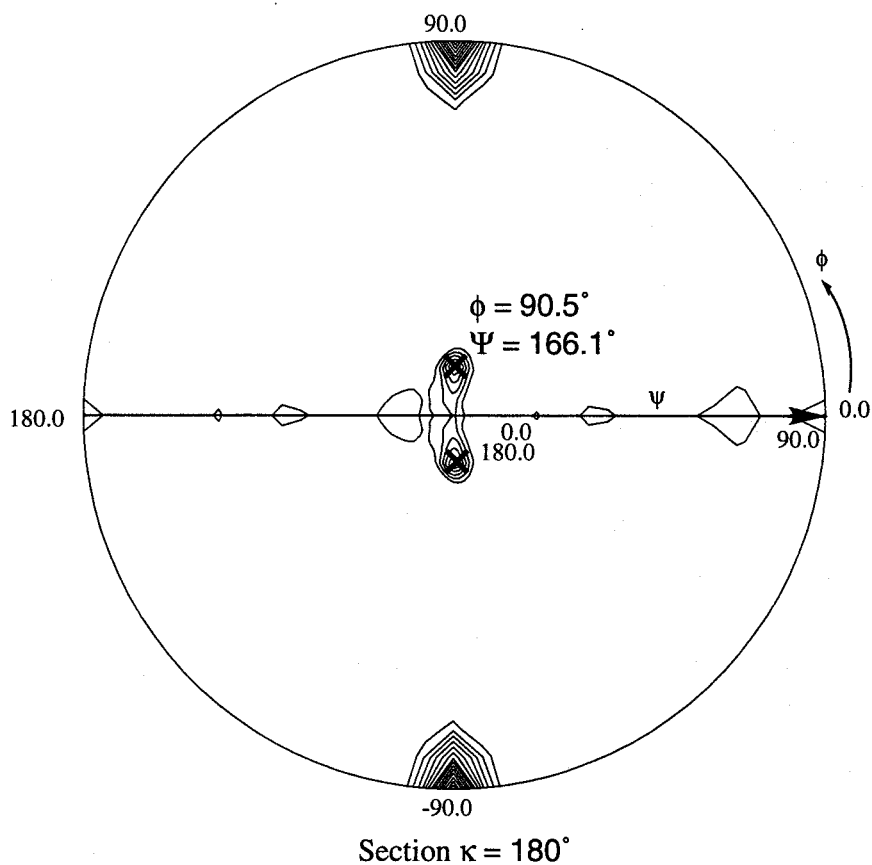
Figure 2-9. A stereographic projection of the κ = 180° section of the self-rotation function of the diffraction data of the crystals of Cys-free Asparagine Synthetase. The section was calculated using the program POLARFFN with data from 10 to 3.5 Å resolution and a Patterson cutoff radius of 20 Å. The position of the cross (×) shows the non-crystallographic two-fold axis; φ = 90.5°, ψ = 166.1°.

CHAPTER 3

Crystal Structure of Asparagine Synthetase

3 - 1. Introduction

The determination of a crystal structure of proteins is dependent on whether or not the phases of the diffraction data is determined by multiple isomorphous replacement (MIR). For phase determination by MIR, the derivative crystals in which heavy atoms are incorporated are needed. The derivative crystals are prepared by soaking the native crystals into a solution containing various heavy atom reagents. At least two different isomorphous derivatives are needed to determine the phase unambiguously. The preparation of the heavy atom derivatives is usually a trial and error process by changing the reagents, concentration of the reagents, soaking time, and pH. The positions of the heavy atoms are determined by the diffraction intensity data of the native and derivative crystals by using the Patterson function. The phases of the diffraction data of the native crystal are then calculated by using these positions of the heavy atom. Electron density of the protein is given by the Fourier transform of the diffraction data including the amplitudes and the phases of the native crystal. The structure models of the protein are then built based on the electron density. Then the refinement of the model obtained is carried out with molecular dynamics. The refinement is a process adjusting the model to find a closer agreement between the observed structure factors ($|F_o|$) and the calculated values ($|F_c|$). The agreement index is usually represented by an R-factor;

$$R\ (\%) = 100 \times \Sigma ||F_o|-|F_c|| / \Sigma |F_o|.$$

The R-factor of the refined protein model usually shows about 20 %.

By the use of the crystals of the Cys-free AS-A obtained as described in Chapter 2, two types of the derivative crystals of the Cys-free AS-A crystals were obtained by screening the soaking conditions using various heavy atom reagents. Since the electron density of AS-A obtained by MIR using the two heavy atom derivative crystals, the models of AS-A was easily constructed. The structure model of AS-A showed an R-factor of 15.4 % at 2.5 Å resolution. The structure of AS-A determined by MIR consisted of the eight-stranded β-sheet flanked by two α-helices, and the binding site of L-Asn was identified. The overall structure of AS-A was found to be similar to the catalytic domain of Aspartyl-tRNA synthetase (AspRS) from *Saccharomyces cerevisiae*.

In this chapter, the X-ray crystal structure analysis of AS-A are described. In addition, the comparison of the structures of AS-A and AspRS is also described.

3 - 2. Experimental Procedures

Materials

$Sm_2(SO_4)_3$, $Pb(NO_3)_2$ and $Tl(OAc)$ were purchased from Nacalai Tesque (Kyoto, Japan). K_2PtCl_4 and $K_2Pt(CN)_4$ were obtained from Aldrich (Milwaukee, USA). $KAu(CN)_2$ and $Hg(OAc)_2$ were purchased from Wako Pure Chemical Industries, Ltd. (Osaka, Japan). Ethylmercurithiosalicylic acid sodium salt (EMTS) and p-chloromercuri benzene sulfonic acid sodium salt (PCMBS)   were purchased from Sigma (St. Louis., USA). Ethylmercuri phosphate (EMP) was a gift from Professor Gregory A. Petsko at Brendeis Univ., USA.

Preparation of Heavy Atom Derivatives

The Cys-free AS-A crystals (native crystals) were prepared as described in Chapter 2. Since the solution for the crystallization contained 5 mM β-mercaptoethanol, the native crystals were transferred three times to a solution [50 mM HEPES (pH7.5), 56 % saturated ammonium sulfate, 10% glycerol, 15 mM $MgCl_2$, and 15 mM L-Asn] in order to remove β-mercaptoethanol. The heavy atom derivative crystals were prepared by soaking the native crystals into a solution containing a heavy metal reagent. The soaking conditions are summarized in Table 3-1. The quality of the heavy atom derivatives of the protein crystals was checked by X-ray diffraction analysis by measuring the intensity data and calculating the difference Patterson map.

X-ray Diffraction Data Collection

The intensity data sets of the native and the heavy atom derivative crystals were collected with RIGAKU R-AXIS IIc imaging plate system mounted on a RU-300 (Rigaku, Tokyo, Japan) operated at 40 kV and 100 mA (λ = 1.5418Å). The intensity data sets were processed with an R-AXIS IIc software (Sato et al., 1992). The conditions of data collection and the statistics of data sets for phasing are shown in Table 3-2.

Table 3-1. List of the reagents checked for the heavy atom derivatives.

Reagents	Concentration (mM)	Soaking time	
$KAu(CN)_2$	4.5	41	hours
K_2PtCl_4	5.0	2	days
K_2PtCl_6	2.0	5	days
$K_2Pt(CN)_4$	1.0	3.5	days
$K_2Pt(CN)_4$ (pH8.0)[¶]	3.2	18	days
EMP	1.0	5.5	days
EMTS	0.8	3	days
$Hg(OAc)_2$	0.2	17	hours
PCMBS	0.5	4.5	days
PCMBS (pH8.6)	1.5	4	days
$Sm_2(SO_4)_3$[¶]	3.5	3.5	days
$Pb(NO_3)_2$	saturated	3.5	days
Tl(OAc)	1.7	2.5	days

EMP : Ethylmercury phosphate
EMTS : Ethylmercurithiosalicylic acid
PCMBS : p-Chloromercuri benzene sulphonic acid
[¶]The reagents used for MIR phasing.

Table 3-2. Summary of data collection and statistics.

	Native	$Sm_2(SO_4)_3$	$K_2Pt(CN)_4$
Camera length (mm)	100.0	100.0	100.0
Spindle axis	-a*	-b*	+b*
Oscillation angle (degree / frame)	1.5	2.0	2.0
Exposing time (min. / frame)	20	30	25
No. of photos	92	91	90
Resolution (Å)	2.5	2.7	2.7
R_{merge} (%)[¶]	10.45	9.12	10.00
Accepted reflections ($I > 1\sigma$ (I))	50944	53981	49797
Unique reflections ($I > 1\sigma$ (I))	17805	15999	15677
Completeness (%)	73.8	83.7	81.6
Completeness for outer shell (%)	54.5 (2.6 - 2.5 Å)	71.6 (2.8 - 2.7 Å)	68.2 (2.8 - 2.7 Å)
Temperature (°C)	20	20	-20[#]
Heavy atom conc. (mM)		3.5	3.2
Soaking time (day)		3.5	18
R_{iso} (%)[§]		6.9	9.3

$$R_{Iso} = \frac{\sum |I_{PH} - I_P|}{\sum (I_{PH} + I_P)}$$

$$R_{merge} = \frac{\sum \sum |\langle I_{h,i} \rangle - I_{h,i}|}{\sum \sum I_{h,i}}$$

[#]The derivative crystal was cooled by FTS.

Phase Determination and Improvement

Phase determination was carried out by the method of multiple isomorphous replacement (Green *et al.*, 1954) and anomalous scattering techniques (Bijvoet, 1954) (MIRAS), and the phase were improved by solvent flattening(Wang, 1985; Leslie, 1987) and molecular averaging with non-crystallographic symmetry (Bricogne, 1976). All procedures for phase calculation and refinement were performed by the program package PHASES (Furey *et al.*, 1996).

The positions of heavy atom were determined by difference Patterson and difference Fourier method. The Harker section ($v = 1/2$) of the difference Patterson map at 5Å resolution showed that the two types of the heavy atom derivative crystals [$Sm_2(SO_4)_3$ and $K_2Pt(CN)_4$] were useful (Figure 3-1). Each of the Harker section indicated two samarium and two platinum sites in an asymmetric unit. Difference Fourier maps did not show the other minor heavy atom binding site. The positions and the occupancies of the heavy atoms were refined with the program PHASIT by using 14474 independent reflections [$F > 2\sigma(F)$] in the resolution range ∞ - 2.7 Å. The isomorphous and anomalous diffraction data to 2.7 Å resolution of samarium derivative were used for phase determination. For the platinum derivative the isomorphous diffraction data to 2.7 Å resolution and the anomalous diffraction data to 3.9 Å were used for phase determination. The diffraction data used were over 1.0 for the phasing power as shown in Table 3-4. When the refinement was carried out, the temperature factors were fixed at 15.0 $Å^2$ for isomorphous data and 5.0 $Å^2$ for anomalous data. The refined heavy atom parameters and the phasing statistics are shown in Table 3-3 and Table 3-4, respectively.

The phases calculated by the isomorphous and anomalous diffraction data were improved by the solvent flattening according to Wang's method, (Wang, 1985; Leslie, 1987) and the solvent fraction was set to 35 %. The phase was further improved by the molecular averaging (Bricogne, 1976) because non-crystallographic two-fold axis ($\phi = 90.5°$, $\psi = 166.1°$, $\kappa = 180.0°$) showed that a dimer exists in the asymmetric units as described in Chapter 2. After 100 cycles of refinement of the non-crystallographic two-fold axis was carried out with the program LSQLOT, the correlation coefficient became 0.62 when sphere radius was 25 Å. Molecular averaging by the refined non-crystallographic two-fold axis was carried out by using 15072 reflections [$F > 1\sigma(F)$]. The procedures of solvent flattening and molecular averaging were performed by the shell script "doall.sh" and "extndavg.sh" (Appendix) included in the program package PHASES, respectively.

(a) $Sm_2(SO_4)_3$ Isomorphous

(b) $Sm_2(SO_4)_3$ Anomalous

(c) $K_2Pt(CN)_4$ Isomorphous
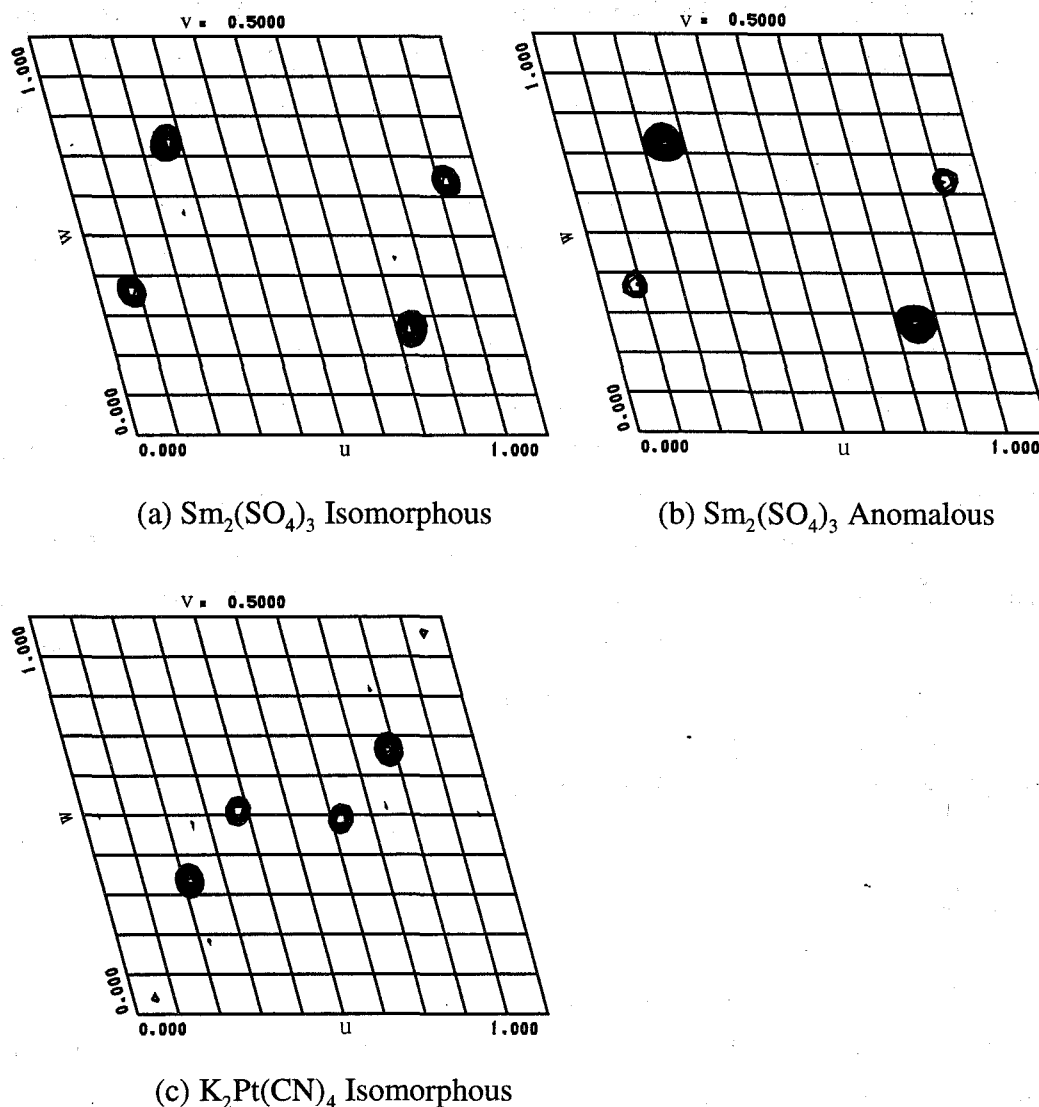
Figure 3-1. The Harker sections of difference Patterson maps of each of the heavy atom derivatives. (a) $Sm_2(SO_4)_3$ derivative isomorphous. (b) $Sm_2(SO_4)_3$ derivative anomalous. (c) $K_2Pt(CN)_4$ derivative isomorphous. $K_2Pt(CN)_4$ derivative could not show strong peaks for anomalous. The Harker section is $v = 0.5$. Sigma cutoff is 3 sigma.

Model Building and Structure Refinement

Main chain and side chain models were built manually into the solvent-flattened and averaged electron-density map on a work station Iris 4D with the program TURBO-FRODO (Jones *et al.*, 1991). The first model of the structure contained 654 residues out of 660 in the dimer molecule. Crystallographic refinement was carried out with the program X-PLOR version 3.1 (Brünger *et al.*, 1987; Brünger, 1992b) using the parameters developed by Engh & Huber. (Engh *et al.*, 1991) At first the refinement was carried out with slow cooling protocol (Brünger *et al.*, 1990) by simulated annealing

(Kirkpatrick *et al.*, 1983) for 14474 reflections in the range of 10 - 2.7 Å [$F > 2\sigma(F)$]. L-Asn and water molecules were then added. Manual model re-building and the positional refinement of the models were carried out, alternatively. The manual model re-building was performed by inspecting $F_o\text{-}F_c$ and $2F_o\text{-}F_c$ map on the program TURBO-FRODO, and the positional refinement was performed by using 17241 reflections in the range of 10 - 2.5 Å [$F > 2\sigma(F)$] with the program X-PLOR.

Sequence Alignment and Structure Comparison between AS-A and AspRS

At first the structure models of Aspartyl-tRNA synthetase from *Saccharomyces cerevisiae* (scAspRS) (Ruff *et al.*, 1991; Cavarelli *et al.*, 1994) ; (PDB code: 1asz) and AS-A were superimposed manually based primarily on the Cα atoms of the secondary structure of these crystal structures by using the program TURBO-FRODO. The sequences of AS-A and scAspRS are manually aligned based on the superimposed structures. Atomic coordinates for the structure comparison were picked up manually based on the sequence alignment. The superposition and the calculation of root-mean-square deviations were carried out by using the command COMPARE and DEVIATION of the program TURBO-FRODO.

3 - 3. Results

Structure Determination and Refinement

As described in Chapter 2, the Cys-free AS-A crystals complexed with L-Asn have been obtained by sitting drop vapour diffusion method. The crystals obtained belonged to a space group of $P2_1$ with cell dimensions a = 52.9 Å, b = 126.2 Å, c = 52.8 Å, β = 105.3°. The author carried out screening of the isomorphous derivative crystals including the heavy atom reagents in order to determine the crystal structure of AS-A by MIR. Two heavy atom derivatives of samarium and platinum were successfully prepared as a result of searching the soaking conditions with various metals (Table 3-1). The native diffraction data set and the heavy atom derivatives data set were collected at Rigaku R-AXIS IIc to 2.5 and 2.7 Å resolution, respectively. The statistics for X-ray diffraction data collection are listed in Table 3-2. As shown in Figure 3-1, the each isomorphous difference Patterson maps for the samarium and platinum data showed that there were two binding sites of the heavy atom in the asymmetric unit for each derivatives. At first, the positions of each heavy atom were determined by using the difference Patterson map: Sm1(0.381, 0.123, 0.137) and Sm2(0.955, 0.407, 0.320); Pt1(0.476, 0.187, 0.239) and Pt2(0.894, 0.332, 0.331). The anomalous difference

Patterson map for samarium showed the identical positions with the isomorphous difference Patterson map. On the other hand, the anomalous difference Patterson map for platinum did not show the peaks. The phases yielded a figure of merit of 0.60 calculated by the multiple isomorphous replacement method and the anomalous scattering techniques (MIRAS). The heavy atom positions were refined and finally determined as: Sm1(0.373, 0.123, 0.139) and Sm2(0.960, 0.409, 0.319); Pt1(0.475, 0.187, 0.239) and Pt2(0.891, 0.332, 0.330). The refined heavy atom parameters and the phasing statistics are shown in Table 3-3 and Table 3-4, respectively. The electron density map at 2.7 Å resolution calculated by MIRAS clearly showed the secondary structure, but the connection of the main chain was still slightly ambiguous. The phase was therefore improved was performed by molecular averaging with non-crystallographic symmetry followed by solvent flattening, and the phases improved showed a figure of merit of 0.83 for 15072 reflections $[F > 1\sigma(F)]$. A lower setting value (35 %) compared to the ideal value (47%) of the solvent region was effective for improving the electron density map so as to keep the electron density of protein for this crystal. The calculated electron density map was easily interpretable for main-chain tracing and model building on the program TURBO-FRODO.

Table 3-3. Refined heavy atom parameters.

Derivative	Site	x	y	z	O	B	Res.	P.P.	R_{K}	R_{C}
Sm iso	Sm1	0.373	0.123	0.139	1.09	15.0	2.7	2.07	0.082	0.66
	Sm2	0.960	0.409	0.319	0.89	15.0				
Sm ano	Sm1	0.372	0.123	0.138	1.11	5.0	2.7	2.28	0.086	
	Sm2	0.961	0.409	0.320	0.89	5.0				
Pt iso	Pt1	0.475	0.187	0.239	1.00	15.0	2.7	1.39	0.14	0.71
	Pt2	0.891	0.332	0.330	0.97	15.0				
Pt ano	Pt1	0.478	0.186	0.237	0.85	5.0	3.9	1.19	0.14	
	Pt2	0.890	0.333	0.327	0.95	5.0				

x, y, z : Fractional coordinate. O : Occupancy.
B : Temperature factor (Å^2). Res. : Resolution (Å).

$$\text{P.P. (Phasing Power)} = \frac{\sum |F_{\mathrm{H}}|}{\sum \left\| F_{\mathrm{PHobs}} | - | F_{\mathrm{PHcalc}} \right\|}$$

$$R_{\mathrm{Kiso}} = \frac{\sum \left\| F_{\mathrm{PH}} | - | F_{\mathrm{P}} + F_{\mathrm{Hcalc}} \right\|}{\sum |F_{\mathrm{PH}}|}$$

$$R_{\mathrm{Kano}} = \frac{\sum \left(\left| |F^+_{\mathrm{PHobs}}| - |F^+_{\mathrm{PHcalc}}| \right| + \left| |F^-_{\mathrm{PHobs}}| - |F^-_{\mathrm{PHcalc}}| \right| \right)}{\sum \left(|F^+_{\mathrm{PHobs}}| + |F^-_{\mathrm{PHobs}}| \right)}$$

$$R_{\mathrm{C}} = \frac{\sum \left| |F_{\mathrm{PHobs}} \pm F_{\mathrm{Pobs}}| - F_{\mathrm{Hcalc}} \right|}{\sum |F_{\mathrm{PHobs}} \pm F_{\mathrm{Pobs}}|}$$

The model was refined by the slow cooling protocol according to the program X-PLOR version 3.1, and the crystallographic R-factor decreased from 41.2 % to 18.7 %. After four cycles of model rebuilding and the positional refinement, the R-factor became 15.4 % for 17241 reflections in the range of 10 - 2.5 Å $[F > 2\sigma(F)]$. The free R-factor (Brünger, 1992a) was 24.4 % based on the randomly selected reflections (10 % of the total) with $F > 2\sigma(F)$. The root mean square deviation of the bond lengths, bond angles, and torsion angles from the standard values were 0.009 Å, 1.2° and 27°, respectively. The current model for each monomer includes 327 residues out of 330, along with an asparagine as a ligand bound to the active site. The total of 84 water molecules were placed in an asymmetric unit. The average temperature factor for all protein was 11.5 Å. The statistics of the refinement are summarized in Table 3-6.

Table 3-4. Summary of phasing statistics.

(a) $Sm_2(SO_4)_3$ Isomorphous

D =	9.30	P.P.=	2.66	M.B.=	91.6	REF.=	1390
D =	5.48	P.P.=	2.69	M.B.=	93.1	REF.=	1390
D =	4.57	P.P.=	2.08	M.B.=	94.3	REF.=	1390
D =	4.07	P.P.=	1.98	M.B.=	93.1	REF.=	1390
D =	3.73	P.P.=	1.99	M.B.=	90.5	REF.=	1390
D =	3.47	P.P.=	1.93	M.B.=	92.5	REF.=	1390
D =	3.26	P.P.=	2.01	M.B.=	94.1	REF.=	1390
D =	3.08	P.P.=	1.91	M.B.=	96.6	REF.=	1390
D =	2.91	P.P.=	1.69	M.B.=	94.3	REF.=	1390
D =	2.77	P.P.=	1.75	M.B.=	97.7	REF.=	1390
D =	2.70	P.P.=	1.80	M.B.=	87.8	REF.=	6
D = ∞-2.70		P.P.=	2.07	M.B.=	93.8	REF.=	13906
		<m> =	0.34	M.R.E.=	0.50		

(b) $Sm_2(SO_4)_3$ Anomalous

D =	9.11	P.P.=	3.19	M.B.=	87.0	REF.=	1362
D =	5.43	P.P.=	2.71	M.B.=	86.9	REF.=	1362
D =	4.55	P.P.=	2.40	M.B.=	88.0	REF.=	1362
D =	4.05	P.P.=	2.25	M.B.=	87.7	REF.=	1362
D =	3.72	P.P.=	2.21	M.B.=	86.1	REF.=	1362
D =	3.46	P.P.=	2.10	M.B.=	88.8	REF.=	1362
D =	3.25	P.P.=	1.92	M.B.=	88.5	REF.=	1362
D =	3.07	P.P.=	2.11	M.B.=	85.7	REF.=	1362
D =	2.91	P.P.=	2.12	M.B.=	89.0	REF.=	1362
D =	2.77	P.P.=	2.11	M.B.=	87.5	REF.=	1362
D =	2.70	P.P.=	0.96	M.B.=	63.3	REF.=	3
D = ∞-2.70		P.P.=	2.28	M.B.=	87.5	REF.=	13623
		<m> =	0.32	M.R.E.=	0.50		

Table 3-4. Continued.

(c) $K_2Pt(CN)_4$ Isomorphous

D = 9.45	P.P.= 2.08	M.B.= 91.0	REF.=	1346
D = 5.51	P.P.= 1.80	M.B.= 86.7	REF.=	1346
D = 4.59	P.P.= 1.45	M.B.= 88.4	REF.=	1346
D = 4.09	P.P.= 1.33	M.B.= 87.9	REF.=	1346
D = 3.75	P.P.= 1.19	M.B.= 86.4	REF.=	1346
D = 3.48	P.P.= 1.25	M.B.= 82.5	REF.=	1346
D = 3.27	P.P.= 1.25	M.B.= 84.9	REF.=	1346
D = 3.08	P.P.= 1.26	M.B.= 87.8	REF.=	1346
D = 2.92	P.P.= 1.20	M.B.= 86.0	REF.=	1346
D = 2.77	P.P.= 1.20	M.B.= 85.9	REF.=	1346
D = 2.70	P.P.= 2.69	M.B.= 89.0	REF.=	4
D = ∞-2.70	P.P.= 1.39	M.B.= 86.7	REF.=	13464
	<m> = 0.27	M.R.E.= 0.49		

(d) $K_2Pt(CN)_4$ Anomalous

D = 12.47	P.P.= 1.64	M.B. = 89.2	REF.=	524
D = 7.48	P.P.= 1.36	M.B. = 85.3	REF.=	524
D = 6.25	P.P.= 1.35	M.B. = 89.9	REF.=	524
D = 5.57	P.P.= 1.21	M.B. = 86.7	REF.=	524
D = 5.11	P.P.= 1.16	M.B. = 90.6	REF.=	524
D = 4.77	P.P.= 1.10	M.B. = 90.3	REF.=	524
D = 4.51	P.P.= 1.14	M.B. = 87.6	REF.=	524
D = 4.30	P.P.= 1.06	M.B. = 90.1	REF.=	524
D = 4.12	P.P.= 1.03	M.B. = 89.4	REF.=	524
D = 3.97	P.P.= 1.08	M.B. = 88.7	REF.=	524
D = 3.90	P.P.= 0.54	M.B. = 51.0	REF.=	2
D = ∞-3.90	P.P.= 1.19	M.B. = 88.8	REF.=	5242
	<m> = 0.24	M.R.E.= 0.50		

D: Resolution range. REF: No. of reflections.

$$\text{P.P. (Phasing Power)} = \frac{\sum |F_H|}{\sum \left| |F_{PHobs}| - |F_{PHcalc}| \right|}$$

$$< m > \text{ (Figure of merit)} = \frac{|F(\text{hkl})_{best}|}{|F(\text{hkl})|}$$

$$\text{M.R.E. (Mean relative error)} = \frac{1}{N} \sum \frac{\varepsilon(\alpha)^2}{2E^2} \quad ; \quad \varepsilon = F_{PHobs} - F_{PHcalc}, \quad E = |F_{PH} \pm F_P| - F_H$$

M.B. (Mean bias) should be 90 degrees for each data set, because there should be no correlation between true protein and heavy atom derivatives.

Table 3-5. Mean figure of merit after each steps.

Phasing step	$<m>$	Reflections
MIR	0.60	14474 $(F>2\sigma(F))$
Molecular averaging	0.83	15072 $(F>1\sigma(F))$

$$< m > \text{(Figure of merit)} = \frac{\left|F(\text{hkl})_{\text{best}}\right|}{\left|F(\text{hkl})\right|}$$

Table 3-6. Summary of refinement of the binary complex of the Cys-free Asparagine Synthetase with L-Asn.

Resolution (Å)	10.0-2.5
Reflections $(F>2\ \sigma(F))$	17421
No. of protein atoms	5118
No. of ligand atoms	18
No. of solvents	84
R_{cryst} (%)	15.4
R_{free} (%)	24.4
R.m.s. bond length (Å)	0.009
bond angle (degree)	1.22
dihedral (degree)	26.8
improper (degree)	2.1
Average B-factor of enzyme (Å^2)	11.5
ligand (Å^2)	22.3
solvent (Å^2)	15.3

$R_{cryst} = 100 \times \Sigma |F_o - F_c| / \Sigma |F_o|$

R_{free} was calculated using 10 % data chosen randomly and omitted from the refinement.

Subunit Structure

Each monomer has a molecular weight of 37 kDa and consists of 330 amino acid residues. The crystal structure of a subunit AS-A complexed with L-Asn is shown in Figure 3-2. Each subunit consisted of a single domain which was composed of eleven α-helices and eleven β-strands. The first three amino acids showed no electron density and was presumed to be disordered in the crystals. The central region was an eight-stranded β-sheet which consisted of six strands running antiparallel to the neighboring strands (β5-β6 and β8-β11) and of the two external parallel strands (β1 and β7). Two antiparallel long α helices (α1 and α3) flanked on a side of the central β-sheet. Three-stranded antiparallel β-sheet (β2-β4) and three α-helices (α2, α4 and α5) located on the opposite side of the central β-sheet. The central β-sheet was surrounded by six α-helices (α6-α11). The β-strands, β6, β10 and β11 were bent at the position of the residues Asp118, Ser251 and Gly294, respectively. The residues assigned as being on α-helix or β-strand are summarized in Table 3-7. The interactions between the main-chain amide and carbonyl groups found in the central eight-stranded β-sheet and three-stranded antiparallel β-sheet are shown in Figure 3-3. The distribution of torsion angles (Ramachandran Plot) of the structure was calculated by the program PROCHECK (Laskowski, 1993) and is shown in Figure 3-4 (Ramachandran *et al.*, 1974). The maximum coordinate error of the AS-A:L-Asn structure was calculated as 0.21 Å estimated by a Luzzati plot (Luzzati, 1952) as shown in Figure 3-5.

Dimer Structure

The overall crystal structure of AS-A was a homo dimer, related to each other by non-crystallographic two-fold axis. The structure of the dimer is shown in Figure 3-6. The three-stranded antiparallel β-sheet from the subunit A (β2-β4) and the same β-sheet from the subunit B (β2'-β4') formed a six-stranded antiparallel β-sheet in the boundary region of the dimer. No interaction between the main-chain amide and carbonyl groups was observed between the strand β3 and β3' in the six-stranded β-sheet. The long helix α1 from one subunit ran antiparallel to the helix α1' from another subunit and slightly interacted with the strand β1' of another subunit. The major polar interactions between the dimer are listed in Table 3-8. A 3464 Å² of the buried surface of the dimeric interface of AS-A included three β-strands (β1, β2 and β3) and the carboxy-terminal amino acid residues between 313 and 319. Ala315 (Cys315 in the wild type) was located in the hydrophobic core. The root mean square difference between each subunit was 0.21 Å for Cα atoms and 0.27 Å for all atoms.
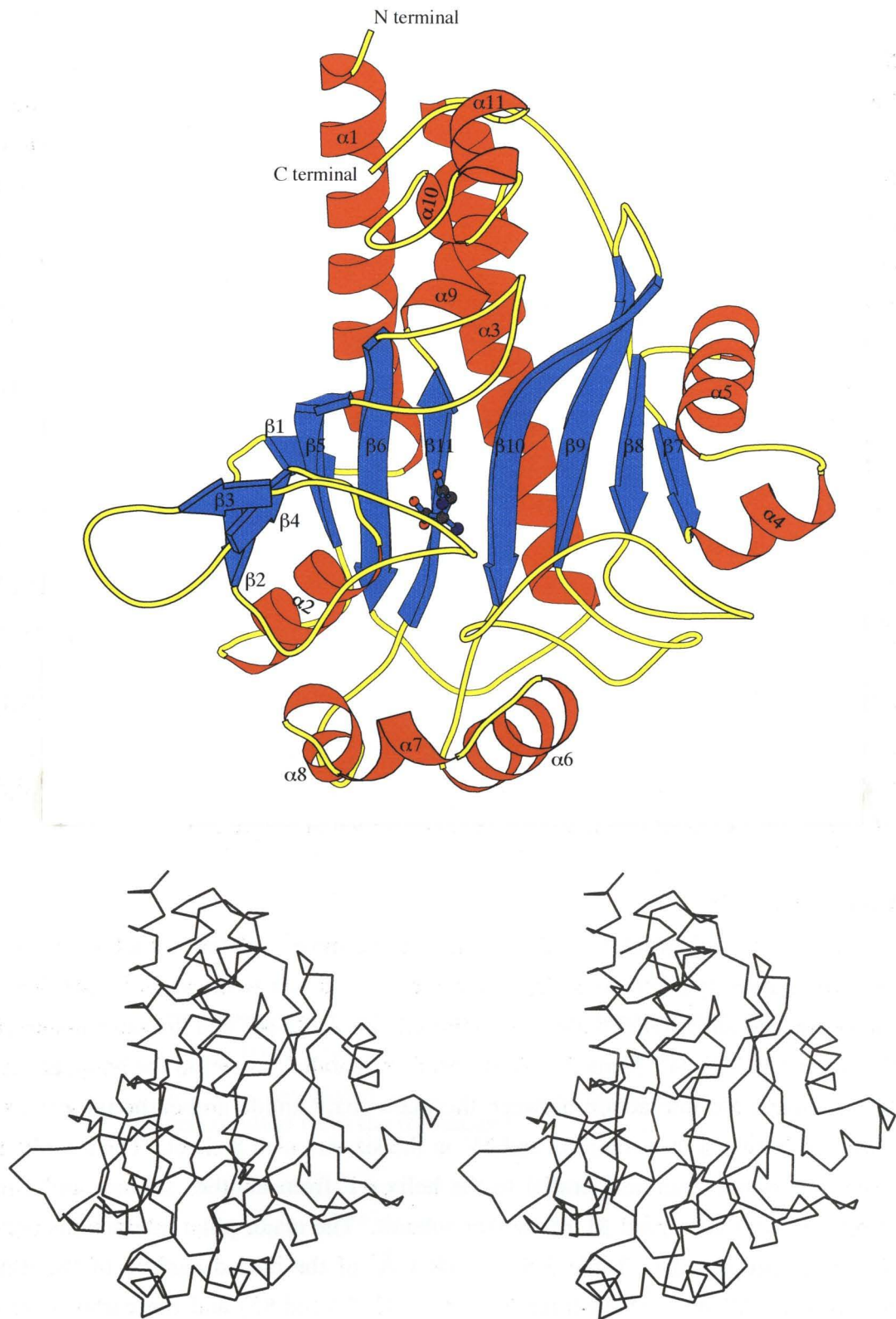
Figure 3-2. Ribbon diagram (upper) and Cα trace stereoview (lower) of the subunit structure of Asparagine Synthetase complexed with L-Asn. The ball-and-stick model shows L-Asn ligand. This is located on the central eight stranded β-sheet.

(a)   (b)
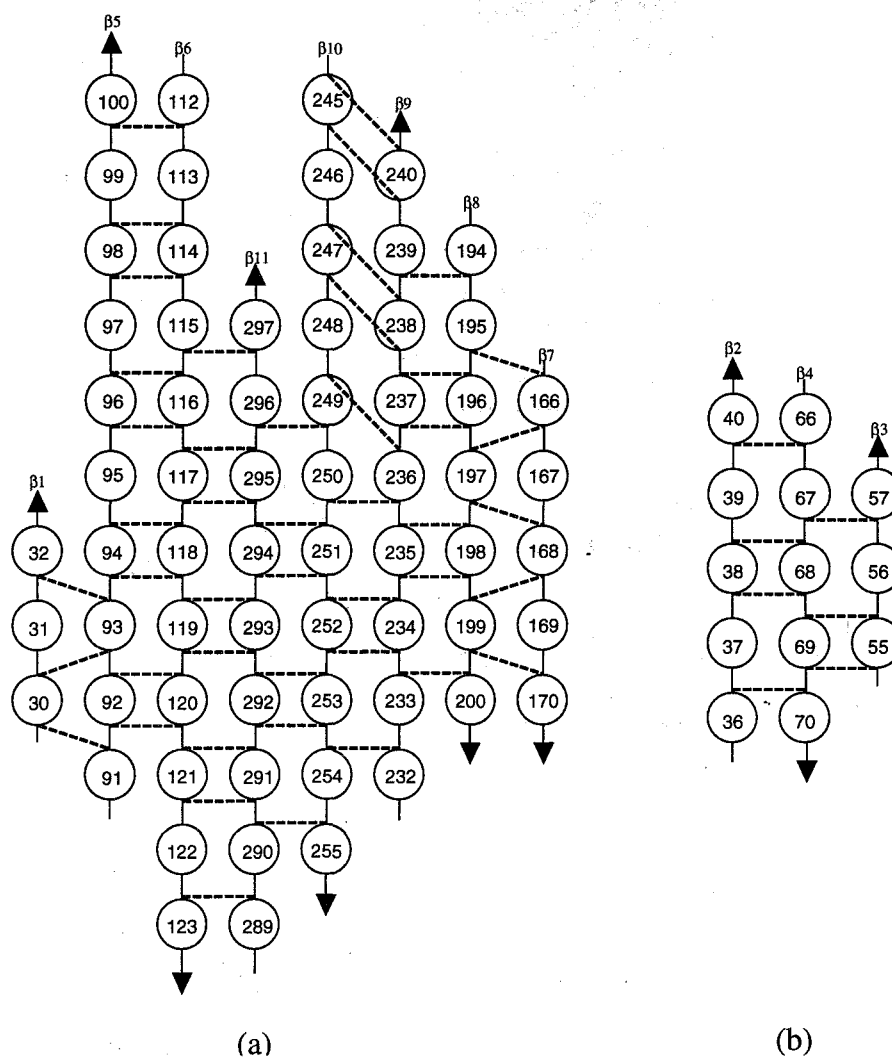
Figure 3-3. Hydrogen bonding network of β-sheets. (a) central eight-stranded β-sheet and (b) three-stranded antiparallel β-sheet of Asparagine Synthetase. A number shows the sequence number of Asparagine Synthetase. Dashed lines show hydrogen bondings.
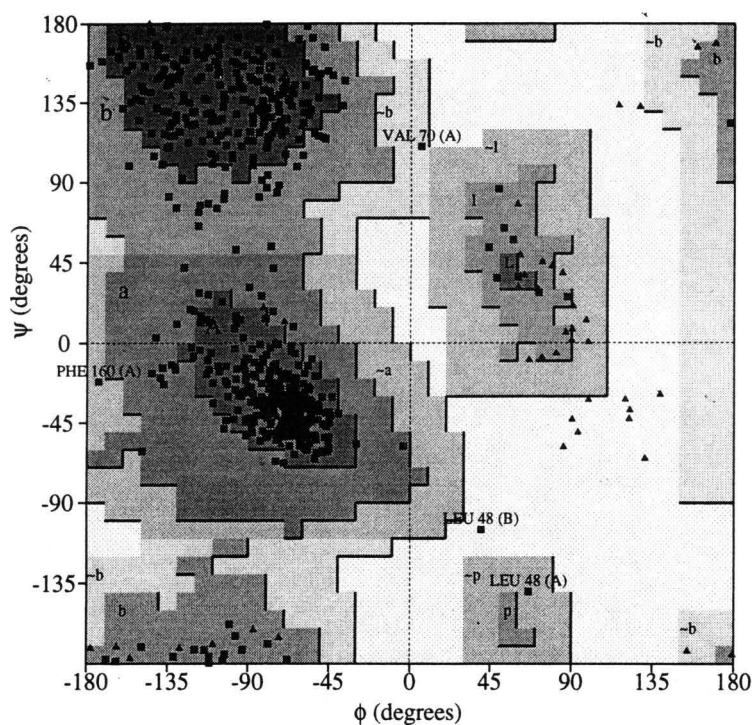
Figure 3-4. Ramachandran plot of the crystal structure of Asparagine Synthetase complexed with L-Asn. The plot was produced with the program PROCHECK. Glycine residues are shown in triangles.
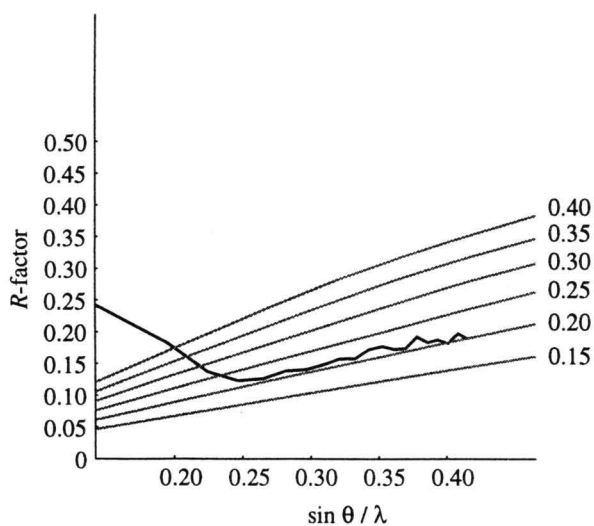
Figure 3-5. Luzzati plot for the refined crystal structure of Asparagine Synthetase complexed with L-Asn. Gray lines are calculated Luzzati lines for coordinate errors. The maximum coordinate error of the binary complex was calculated as 0.21 Å.

Subunit B   Subunit A

Figure 3-6. Ribbon diagram of the dimer structure of Asparagine Synthetase. The non-crystallographic two-fold axis is perpendicular to the plane of this sheet.

Table 3-7. Secondary structure of Asparagine Synthetase.

Helix	Residues		Strand	Residues	
α1	5	-	27	β1	29	-	31
α2	76	-	83	β2	37	-	39
α3	130	-	151	β3	55	-	57
α4	170	-	176	β4	67	-	69
α5	182	-	193	β5	91	-	99
α6	258	-	268	β6	113	-	122
α7	271	-	275	β7	166	-	169
α8	277	-	283	β8	195	-	199
α9	297	-	305	β9	233	-	240
α10	310	-	312	β10	245	-	254
α11	320	-	325	β11	290	-	296

Table 3-8. Polar interactions between subunits.

| Subunit A | | Subunit B | | Distance (Å) |
Residue	Atom	Residue	Atom	
Q 9 A	OE1	- Q 33 B	N	3.03
S 13 A	OG	- E 31 B	OE2	3.06
E 31 A	OE2	- S 13 B	OG	3.42
Q 33 A	N	- Q 9 B	OE1	2.99
K 60 A	N	- P 101 B	O	3.21
K 60 A	NZ	- D 102 B	O	2.98
K 60 A	O	- E 103 B	O	3.05
P 101 A	O	- K 60 B	N	3.15
D 102 A	O	- K 60 B	NZ	2.78
E 103 A	O	- K 60 B	O	3.17

L-Asparagine Binding Site

One L-Asn molecule was found to bind to the subunit of AS-A. The binding site of L-Asn was located on one side of the central eight-stranded β-sheet (Figure 3-2). The L-Asn was incorporated in the network interaction constructed by Arg214, Asp219, Arg255. Glu120, Lys77, Asp118 and Gln116. As shown in Figure 3-7, the polar interactions were observed between the α-carboxyl group of the ligand L-Asn and the side chains of Lys77 and Arg255. The amino group of L-Asn interacted with the main chain amide carbonyl of Ser251 directly and the side chain of Asp219 through a water molecule. The side chain of Asp46 and Gln116 bound to the nitrogen atom and the oxygen atom of the carbamoyl group of L-Asn, respectively.

Figure 3-7. L-Asn binding site of Asparagine Synthetase. L-Asn ligand is illustrated in thick lines. Water molecule is indicated as dot. Dashed lines show the polar interactions.

Comparison of Crystal Structure between AS-A and AspRS

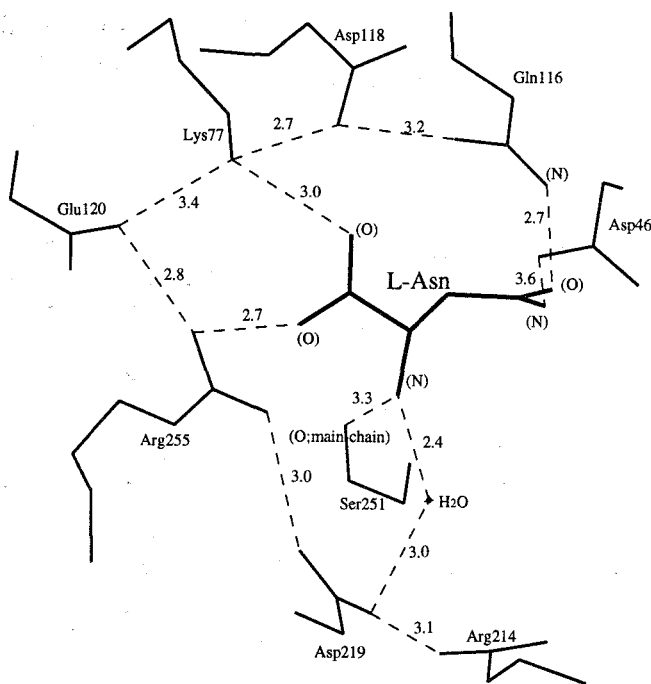The overall structure of AS-A was most similar to the structure of the catalytic domain of aspartyl-tRNA synthetase from *Saccharomyces cerevisiae* (scAspRS) (Ruff *et al.*, 1991) among so far structurally defined class II aminoacyl-tRNA synthetase (aaRS). This is the first example that the fold of the catalytic domain of class II aaRS was detected other than the class II aaRS family. The structures of both enzymes are compared in Figure 3-8. The construction of the secondary structure in both enzymes was almost the same; both comprise eleven β-strands and nine α-helices with identical topology and sequence order as shown in Figure 3-9. The only difference was that AS-A did not have an α3a helix between α3 and α4 helix while scAspRS possessed an α3a helix and did not have two short α helices (α7 and α11). The root mean square differences with respect to the Cα atoms of the whole structure (175 residues) and of the central antiparallel β-sheet (51 residues) between the structure of AS-A and the catalytic domain of scAspRS were calculated as 1.9 Å and 1.1 Å, respectively. These lower values revealed their structural similarity. The drawing of the superimposition of the both structures are shown in Figure 3-10.

Because the structures of both enzymes were similar, the sequences of AS-A and scAspRS were compared based on the superimposed both structures (Figure 3-11). The structure-based sequence alignment identified fifteen conserved residues, and they were all catalytically and structurally important residues of scAspRS. A conserved proline (Pro35 in AS-A, Pro273 in scAspRS) among the identical residues was located on the dimer interface. The other residues detected were existed in or near the central eight-stranded β-sheet. Lys306, Asp342, Glu344, and Arg485 in scAspRS are involved in the recognition of the substrate L-Asp. The corresponding residues of AS-A, Lys77, Asp118, Glu120, and Arg255, were found to be positioned near the bound L-Asn. The Arg100, Asp471, Glu478 and Arg531 of scAspRS are involved in the recognition of ATP. The Ser481 of scAspRS interacts with the carbonyl group of α-aspartyl adenylate intermediate. In the case of AS-A, the amino group of L-Asn bound to the main chain carbonyl of the corresponding residue of Ser251. The short identical motif of ^{524}GGGIG^{528} of scAspRS is located in the β11 strand and is necessary for forming the recognition site of ATP and L-Asp. The corresponding motif ^{292}GGGIG^{296} of AS-A also existed in the β11 strand. Figure 3-10c shows the drawing of the superposition of all the identified residues detected by structurally based sequence alignment. The root mean square differences with these residues between AS-A and scAspRS were calculated as 0.77 Å for α-carbons and 1.0 Å for all atoms, indicating that the structural arrangement of these residues were also similar.

(a) Asparagine Synthetase   (b) Aspartyl-tRNA Synthetase catalytic domain
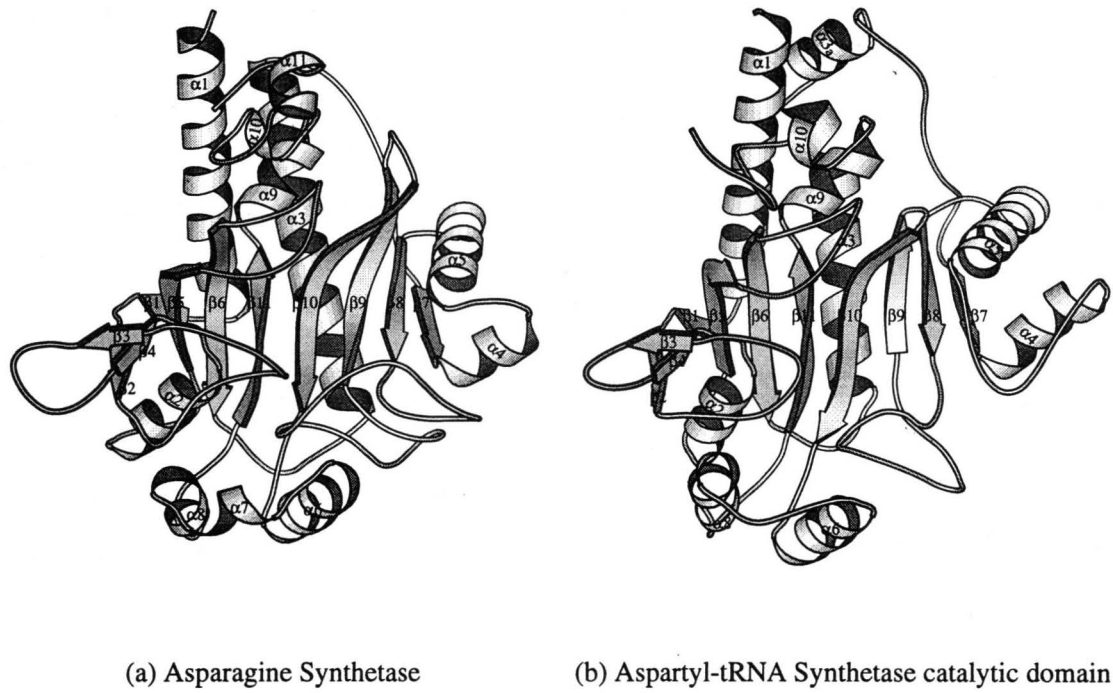
Figure 3-8. Ribbon diagram of (a) Asparagine Synthetase from *Escherichia coli* and (b) the catalytic domain of Aspartyl-tRNA Synthetase from *Saccharomyces cerevisiae*.

(a) Asparagine Synthetase   (b) Aspartyl-tRNA Synthetase catalytic domain
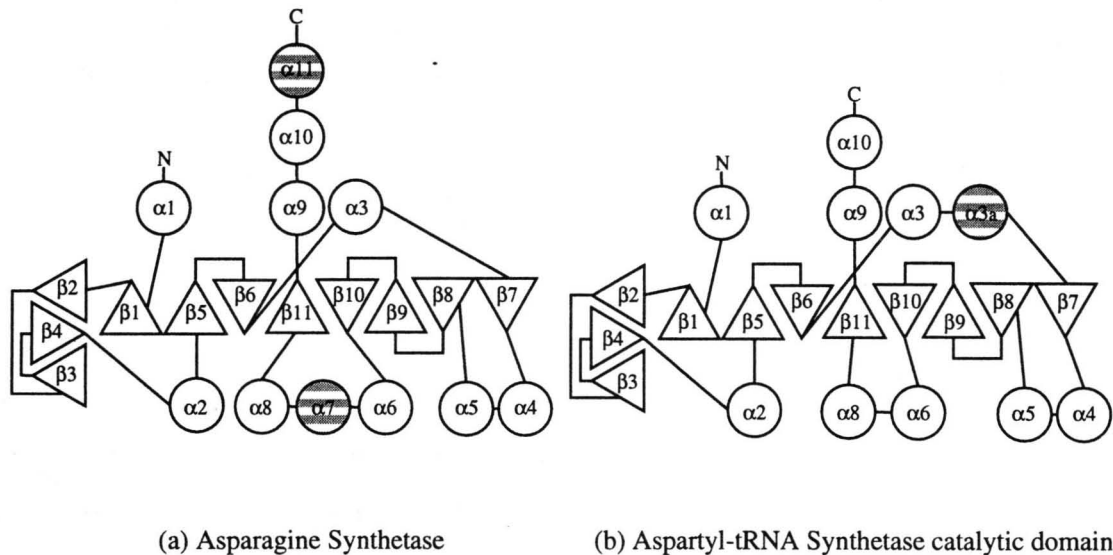
Figure 3-9. Topology of (a) Asparagine Synthetase from *Escherichia coli* and (b) the catalytic domain of Aspartyl-tRNA Synthetase from *Saccharomyces cerevisiae*. Circles and triangles show α-helices and β-strands, respectively. Striped circles show a-helices which don't exist between both structures.

(a) Overall structure

(b) Antiparallel β-sheet

(c) Catalytic residues
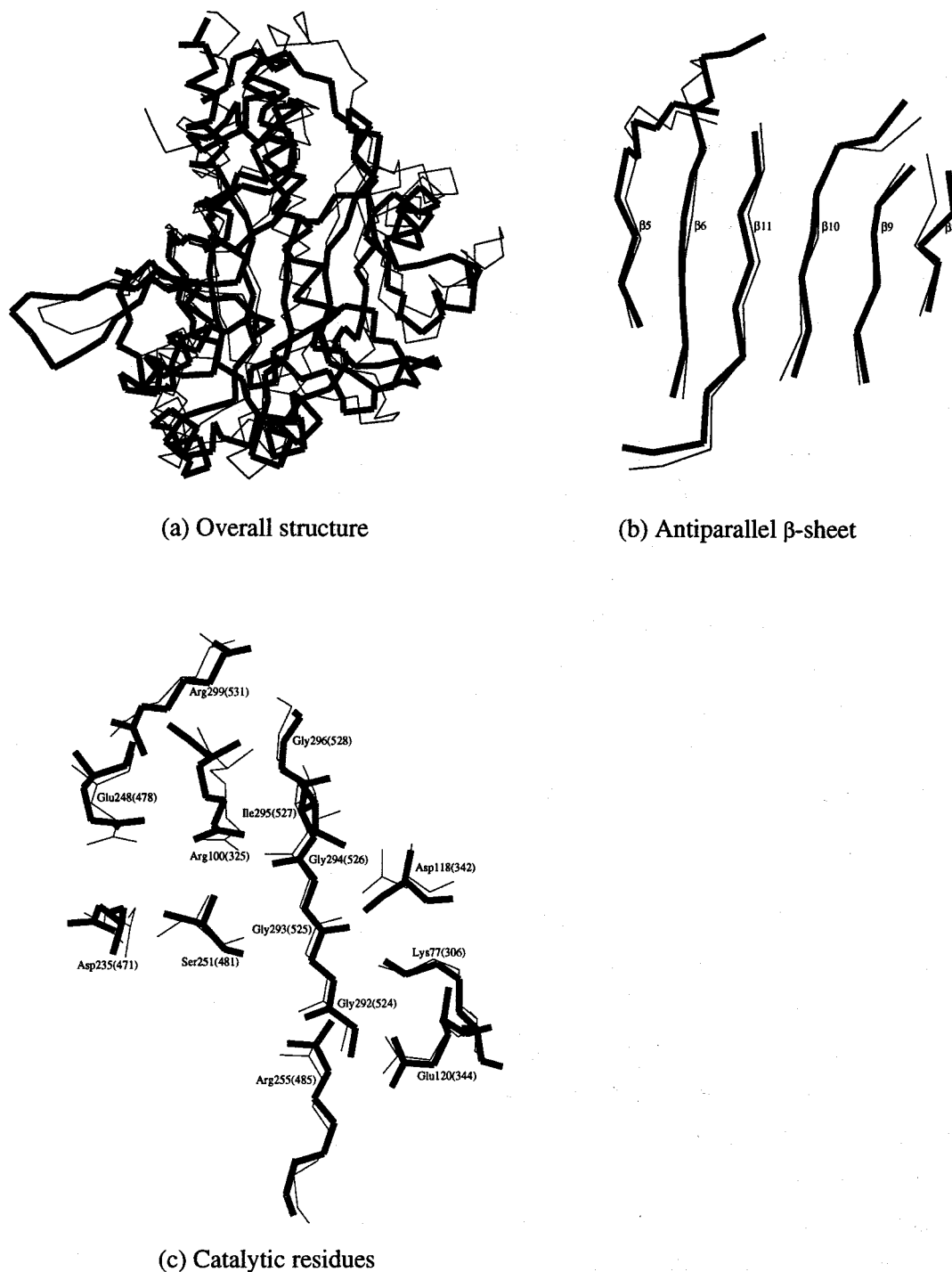
Figure 3-10. Superposition of Asparagine Synthetase and Aspartyl-tRNA Synthetase from *S. cerevisiae* catalytic domain. (a) overall structure, (b) central antiparallel β-sheet, (c) the identical residues detected by the sequence comparison based on the superposition of both enzymes. Thick and thin lines show Asparagine Synthetase and Aspartyl-tRNA Synthetase, respectively. The residue number shows the sequence number of Asparagine Synthetase. The corresponding sequence number of Aspartyl-tRNA Synthetase shows in the parenthesis.

3 - 4. Discussion

Comparison of Crystal Structure between AS-A and AspRS

The three dimensional structure of AS-A was elucidated for the first time. The overall structure comprised a single and compact domain which was consisted of an eight-stranded β-sheet with two long α-helices running along the central region of the β-sheet. This secondary, tertiary and quaternary structures were all strikingly similar to the catalytic domain of scAspRS, although amino acid sequence of AS-A is quite different from that of scAspRS. However, the structure-based sequence alignment (Figure 3-11) identified some amino acids conserved between AS-A and scAspRS. The identified residues were structurally and catalytically important for scAspRS (Cavarelli et al., 1994). It seems therefore that the corresponding residues of AS-A are also structurally and catalytically relevant residues.

The Pro35 of AS-A, while is corresponding to Pro273 of scAspRS, is one of the conserved residue. This proline residue of scAspRS is structurally important as a key residue involved in subunit-subunit interaction (Eriani et al., 1993) and is conserved in most of the class II aaRSs (Eriani et al., 1990; Logan et al., 1995). The Pro273 of one subunit and the carboxy-terminal residues (Phe548, Pro549, Arg550, and Pro557) are involved in the hydrophobic interaction between subunits. In addition the Pro273 is involved in the formation of the hydrogen bonding between subunits. Pro273→Gly mutant resulted in a loss of activity by the disappearance of the hydrogen bonding interactions, suggesting the conformational change of the substrate binding site. The dimeric interaction is a structural prerequisite for the activity of substrate binding region constructed from the eight-stranded central β-sheet (Eriani et al., 1993). And now AS-A is also a homo-dimeric enzyme consists of a homo dimer. The corresponding Pro35 of AS-A was found to be in the subunit-subunit interface. The similar hydrophobic interactions were made of between Pro35 of one subunit and the carboxy-terminal residues (Val313 to Pro319) of the other subunit. While the same hydrogen bonding interaction as in scAspRS was not observed in AS-A, Glu31 and Gln33 close to the Pro35 interacted with Ser13 and Gln9 of the other subunit, respectively. Thus AS-A formed a similar hydrophobic and hydrogen bonding interaction between the subunits to that observed in scAspRS. According to the structural and functional similarity of Pro35 of AS-A and Pro273 of AspRS, it is most likely that Pro35 of AS-A is also indispensable to form the dimer.

```
                α1                    β1        β2                           β3            β4
         <-------------------->     <->       <->                          <->           <->
         1      10       20          30         40         50.        60           70
ecAS-A   MKTAYIAKQRQISFVKSHFSRQLEERLGLIEVQA■ILSRVGVGDGTQDNLSGCEKAVQVKVKALPDAQFEVVHSL
scAspRS  -TVTNQAIFRIQAGVCELFREYLAT-KKFTEVHT■KLLGAPSEGG------SSVFEVTYFK---GKAYLAQSP
         241        250        260         270        280        290          300

              α2              β5                         β6                        α3
          <-------->       <-------->              <-------->          <---------------
          80          90        100        110        120        130        140
ecAS-A   AKW■RQTLGQHDFSAGEGLYTHMKAL■PDEDRLSPLHSVYVDQW■W■RVMGDGERQFSTLKSTVEAIWAGIKA
scAspRS  QFN■QQLIVADFE----RVYEIGPVF■AENS-NTHRHMTEFTGL■M■MAFEEH------YHEVLDTLSELFVF
              310        320        330        340        350          360

         --------->                                 β7      α4                   α5
                                                 <--->   <---->          <----------->
         150                       160        170        180                  190
ecAS-A   TEAAVSEEFGLAP-------------FLPDQIHFVHSQELLSRYPDLD--------AKGRERAIAKDLG--
scAspRS  IFSELPKRFAHEIELVRKQYPVEEFKLPKDGKMVRLTYKEGIEMLRAAGKEIGDFEDLSTENEKFLGKLVRDK
              370        380        390        400        410        420      430

              β8                                         β9          β10          α6
          <---->                                      <------>    <--------->    <----
          200        210        220        230        240        250        260
ecAS-A   ----AVFLVGIGGKLSDGHRHDVRAPDYDDWSTPSELGHAGLNG■ILVWNPVLEDAF■LS■MGI■VD-ADTLK
scAspRS  YDTDFYILDKFPLEIRPFYTMPDPANPKY----------SNSY■FFMR------GE■IL■GAQ■IHDHALLQ
         440        450        460                   470          480        490

                  α7       α8               β11         α9         α10        α11
         ----->  <--->  <------>         <-----><-------->       <->        <---->
         270        280        290        300        310        320        330
ecAS-A   HQLALTGDEDRLE--LEWHQALLRGEMPQT■GGGIG■O■■LTMLLLQLPHIGQVQCGVWPAAVRESVPSLL
scAspRS  ERMKAHGLSPEDPGLKDYCDGFSYG-CPPH■GGGIG■L■■VVMFYLDLKNIRRASLFPRDPKRLRP-----
         500        510        520        530        540        550    557
```
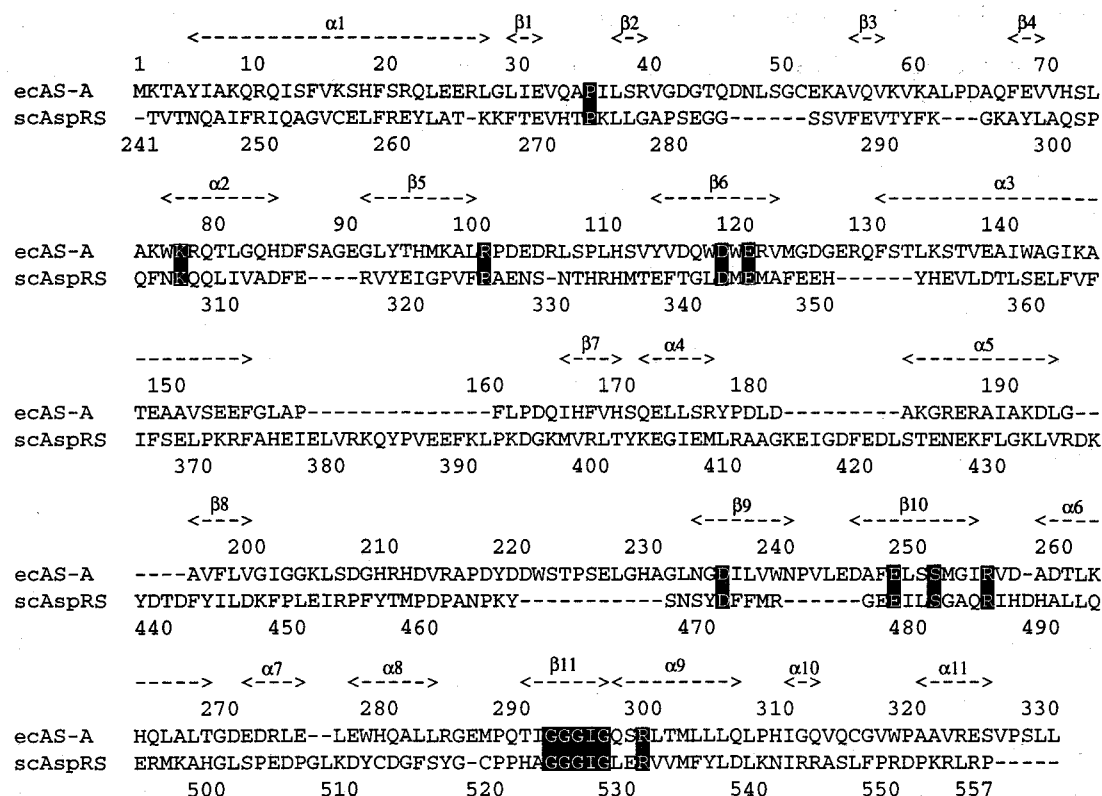
Figure 3-11. Structurally based sequence alignment between Asparagine Synthetase from *E. coli* (ecAS-A) and the catalytic domain of Aspartyl-tRNA Synthetase from *S. cerevisiae* (scAspRS). A number of upper and lower level shows the sequence number of ecAS-A and scAspRS, respectively. Secondary structure shows that of ecAS-A. Black boxes show that the residues of ecAS-A are identical with the structurally and catalytically important residues of scAspRS.

The other conserved residues are catalytically important in terms of the interaction with the substrates; ATP or L-Asp in scAspRS (Cavarelli *et al.*, 1994). ATP and L-Asp are the common substrates of both AS-A and AspRS. In the initial step of the reaction, AS-A and scAspRS form the β- or α-aspartyl adenylate intermediate, respectively, in which the substrate L-Asp is activated as a mixed anhydride with AMP. Lys306, Glu344, and Arg485 in scAspRS are essential for the recognition of β-carboxyl group of the substrate L-Asp and are conserved in all AspRSs of different origin. The β-carboxyl group of L-Asp interacted with Lys306 and Arg485 which were hydrogen-bonded to Glu344 (Cavarelli *et al.*, 1994). It was observed that a similar interaction between the α-carboxyl group of L-Asn and the residues of Lys77 and Arg255 in the structure of AS-A:L-Asn complex. It appears therefore that these residues in AS-A are also necessary for the recognition of the α-carboxyl group of L-Asp substrate. Asp342 of scAspRS is of critical importance for the recognition of amino group of L-Asp since

the residue is hydrogen-bonded to the amino group of the substrate L-Asp, but the corresponding Asp118 of AS-A did not bind the amino group of L-Asn as shown in Figure 3-7. These enzymes seem to be different in terms of the recognition mechanism of the substrate L-Asp, because different aspartyl-adenylate intermediate are formed in the course of the reaction: α-aspartyl adenylate for scAspRS and β-aspartyl-adenylate for AS-A. It seems therefore that the role of Asp118 of AS-A is different from Asp342 of scAspRS for the recognition of the substrate L-Asp, although structure-based sequence alignment identified these residues as conserved ones. Arg325, Asp471, Glu478 and Arg531 of scAspRS among the conserved residues play a role in the positioning of the phosphate group of ATP (Cavarelli et al., 1994). Since the structure of AS-A:ATP complex has not yet been determined, the accurate position of ATP in AS-A is unclear. However, the equivalent four residues were located in almost the same positions between AS-A and scAspRS as shown in Figure 3-10c. In addition, both enzymes share the same reaction mechanism in which the a-phosphate of ATP is attacked by the carboxyl group of L-Asp as the initial step. Assuming that AS-A and scAspRS are similar in the recognition of ATP, the corresponding residues might have the same catalytic role. Arg325 and Arg531 of scAspRS are essential for the recognition of α- and γ-phosphate, respectively, and conserved in all class II aaRSs (Eriani et al., 1990). It is appeared therefore that the corresponding Arg100 and Arg299 of AS-A are important residues for the recognition of ATP. The substitution of the Arg299 with other amino acid, even with a lysine, resulted in a complete loss of catalytic activity of AS-A (Hinchman et al., 1992), indicating the critical role of Arg299 in catalysis. Asp471 and Glu478 of scAspRS indirectly bind β- and γ-phosphate of ATP through Mg^{2+} ion. It seems likely that the corresponding Asp235 and Glu248 of AS-A also interact with the β- and γ-phosphate of ATP through Mg^{2+} ion. Ser481 of scAspRS interacted with the carbonyl group of the α-aspartyl adenylate intermediate. However, it is not clear that the corresponding Ser251 of AS-A plays the same role, since AS-A and scAspRS form the different aspartyl adenylate intermediate. A small conserved motif of GGGIG was found in the β11 of both enzymes. The mutational analysis of Gly526→Ala and Gly528→Ala in scAspRS led to a decrease of the affinity towards L-Asp and ATP, respectively. The residues are not catalytic residues in scAspRS but are necessary to make the catalytic pocket (Cavarelli et al., 1994). It seems that the motif is also necessary to form the binding region of ATP and L-Asp in AS-A.

It was found that the structural similarity between AS-A and scAspRS. Thus both enzymes may have a evolutional relationship. The process of evolution are generally divided into two ways, the divergent evolution and the convergent evolution.

Matthews *et al.*(1981) proposed a series of criteria for distinguishing these evolutional process:

(1) The DNA sequences of their genes are homologous.

(2) The respective amino acid sequences are homologous.

(3) The respective three dimensional structures are homologous.

(4) The respective interactions between enzyme and substrate are homologous.

(5) The respective mechanisms of catalysis are similar.

(6) The segments of the polypeptide chain essential for catalysis are in the same sequence.

The evolution is most likely to be divergent when most of the criteria are met. If few hold true, the convergent evolution is likely. For example the lysozyme from hen egg white and the lysozyme from T4 bacteriophage have no detectable homologies in their amino acid sequences, but the three dimensional structures and the catalytic residues are very similar between both enzymes. In this case the criteria 3 to 6 are met. Thus the divergent evolution is proposed (Matthews *et al.*, 1981). Since DNA or amino acid sequences may easily change compared to the three dimensional structures (Matthews *et al.*, 1985), the conservation of three dimensional structure is most necessary for the divergent evolution. An example of convergent evolution is subtilisin and chymotrypsin. The three dimensional structure and the amino acid sequence of subtilisin are different from that of chymotrypsin. Both enzymes, however are homologous with respect to the enzyme-substrate interaction and catalysis, only criteria 4 and 5 holding true. This appears to be a case of convergent evolution (Robertus *et al.*, 1972). Because the convergent evolution arises from the catalytic necessity, the reaction mechanism and the catalytic residue are the same or similar in spite of the difference of three dimensional structure.

Now let us think about the evolutional relationship between AS-A and scAspRS. Although AS-A and scAspRS have no sequence similarity, structure-based sequence alignment showed that both enzymes are quite similar in the three dimensional structure, the enzyme-substrate interaction, the reaction mechanism, and the catalytic residues, meeting the criteria 3 to 6. This case is similar to that of lysozyme. It is believed that the structure-based sequence alignment is more meaningful for distantly related proteins than an alignment based solely on sequence, because the three dimensional structure of related proteins is more rigorously preserved than either DNA or amino acid sequence (Neidhart *et al.*, 1990). Therefore AS-A and AspRS may be related as a divergent evolution. In addition, the high similarity of the reaction mechanism and the three dimensional structure of both enzymes is consistent with the

41

hypothesis that new enzymatic activities evolve by recruitment of a protein catalyzing the same type of chemical reaction (Petsko *et al.*, 1993; Babbit *et al.*, 1995). These results suggest that AS-A and scAspRS have evolved from a common ancestor.

The crystal structures of AspRS are also determined for prokaryotic AspRS from *Thermus thermophilus* (ttAspRS) (Poterszman *et al.*, 1994). The structure and the catalytic residues of both enzymes are almost identical, but there are two point which are different between both enzymes: the structure of ttAspRS has an insertion domain which located between α4 and α5 of scAspRS, and the conserved motif of GGGIG in eukaryotic AspRS was different with the corresponding sequence (GIAWG) of ttAspRS. AS-A does not have the insertion domain and the small motif of GIAWG of ttAspRS. Therefore AS-A seems to be more similar to eukaryote AspRS than prokaryote AspRS, although AS-A are only distributed in prokaryotes.

Recognition of L-Aspartic Acid Substrate

AS-A and scAspRS form different aspartyl adenylate intermediate in spite of using the same substrate, ATP and L-Asp, in the first reaction step. This means that the recognition mechanism of AS-A for L-Asp is expected to differ from that of scAspRS. The present AS-A crystal structure revealed the details of the L-Asn binding site in the catalytic region, but not of the substrate L-Asp. It is then presumed the binding mechanism of the substrate L-Asp by changing the ligand from L-Asn to L-Asp. Figure 3-12a shows the proposed binding mode of L-Asp in AS-A. The L-Asp binding mechanism of scAspRS established by the structure of scAspRS:ATP:L-Asp:tRNA^{Asp} complex (Cavarelli *et al.*, 1994) is shown in Figure 3-12b. Four residues (Lys77, Asp118, Glu120 and Arg255 of AS-A; Lys306, Asp342, Glu344 and Arg485 of scAspRS) concerning the recognition of the substrate L-Asp were identified by structure-based sequence alignment. The network composed by Lys306, Glu344 and Arg485 of scAspRS interact with the β-carboxyl group of the substrate L-Asp. As to the recognition by AS-A, the α-carboxyl group of the substrate L-Asp is also incorporated into the network of Lys77, Glu120 and Arg255. The binding mechanism of the α-carboxyl group of the substrate L-Asp in AS-A is identical with that of the β-carboxyl group of the substrate L-Asp in scAspRS. Namely the Lys-Glu-Arg network is necessary for the recognition of the carboxyl group of L-Asp. Asp342 of scAspRS forms an electrostatic interaction with the amino group of the substrate L-Asp. Asp118 of AS-A is located in the same position as shown in Figure 3-11 and 12. This residue, however, does not bind to the amino group of L-Asp, but binds to the side chain of Gln116. In AS-A, the amino group of L-Asp interacts with Asp219 and Ser251, both of

which are place on the opposite side of Asp118 of AS-A. The role of Asp118 of AS-A and Asp342 of scAspRS is different in the recognition of L-Asp. Gln303 of scAspRS was hydrogen-bonded to the α-carboxyl group of L-Asp. The corresponding position is occupied by Ala74 in AS-A. Since the Ala74 can not bind to the β-carboxyl group of L-Asp, Gln116 of AS-A instead interacts with the β-carboxyl group. The positions of these glutamine residues (Gln303 in scAspRS, Gln116 in AS-A) are also different in both enzymes. The arrangement of the catalytic residues was slightly different between both enzymes, indicating that the recognition mechanism of the substrate L-Asp of AS-A and scAspRS was different.

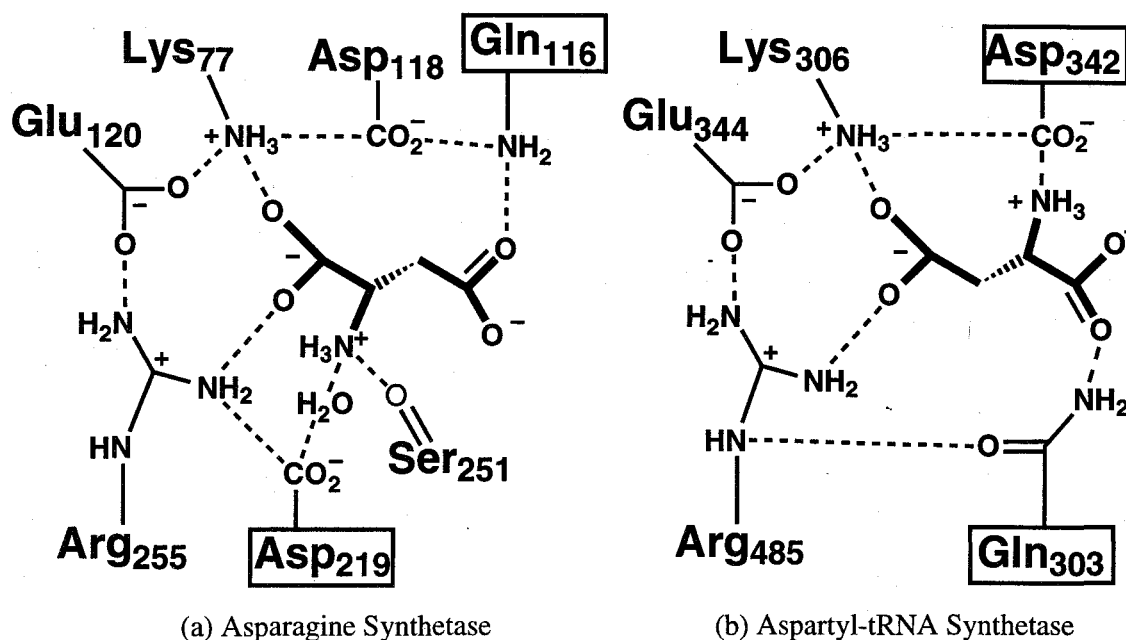(a) Asparagine Synthetase   (b) Aspartyl-tRNA Synthetase

Figure 3-12. Schematic diagram of L-Asp binding site, (a) Asparagine Synthetase, (b) Aspartyl-tRNA Synthetase from *S. cerevisiae*. L-Asp ligand is illustrated in thick lines.

CHAPTER 4

Crystal Structure of Ternary Complex of Asparagine Synthetase with AMP & L-Asn

4 - 1. Introduction

The first step of the reaction mechanism of AS-A which catalyzes the synthesis of L-Asn by two-step reaction, is the formation of β-aspartyl-adenylate intermediate by the nucleophilic attack of the substrate L-Asp. As described in Chapter 3, the binding mechanism of the substrate L-Asp is identified by the binary complex of AS-A with L-Asn, however, ATP binding site has not been clear yet. Thus the author carried out the structure determination of the ternary complex structure of AS-A with AMP and L-Asn at 2.2 Å resolution in order to explicate the binding mechanism of ATP. As the results, the proposed binding mechanism of ATP was found to be similar to that of AspRS. The overall structure of AS-A is also similar to the catalytic domain of AspRS as described in Chapter 3, furthermore, the reaction mechanism of the formation of aspartyl-adenylate can be looked upon similar in both enzymes as shown in Figure 4-1. It was proposed that the formation of β-aspartyl-adenylate intermediate by AS-A passes through in-line mechanism by comparing with the reaction mechanism of α-aspartyl-adenylate intermediate of AspRS which is found by the structural analysis (Cavarelli *et al.*, 1994; Poterszman *et al.*, 1994).
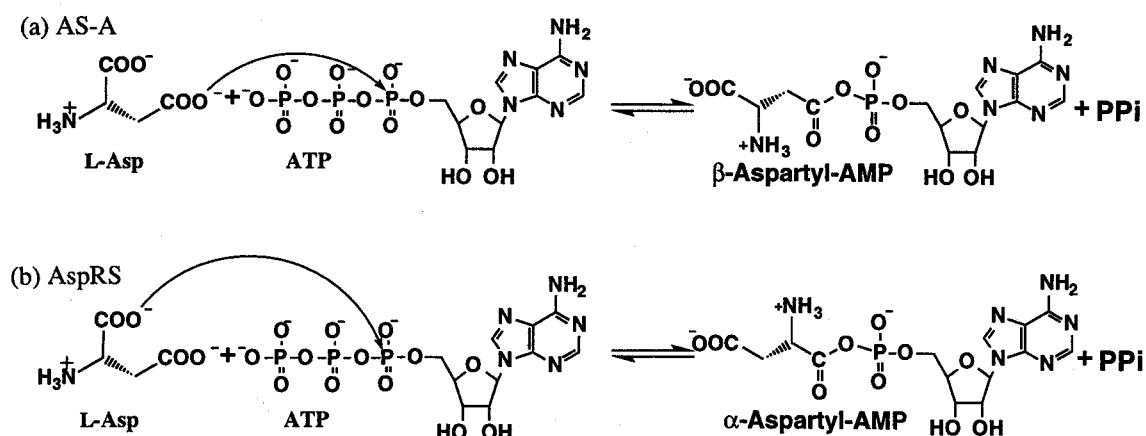

Figure 4-1. The reaction scheme of the formation of aspartyl-adenylate intermediate of (a) Asparagine Synthetase and (b) Aspartyl-tRNA Synthetase.

In this chapter, the binding mechanism of the substrates ATP and L-Asp of AS-A are described. Furthermore, the reaction mechanism of the formation of β-aspartyl-adenylate is described.

4 - 2. Experimental Procedures

Materials

Plasmid pUNAd37Cys-free was used for overproduction of Cys-free AS-A. AMP was purchased from Oriental Yeast Co., Ltd. (Tokyo, Japan). L-Asn was obtained from Wako Pure Chemical Industries, Ltd. (Osaka, Japan). Commercially available chemicals used were of the purest grade.

Preparation of the Ternary Complex of the Cys-free AS-A with AMP and L-Asn

The overexpression and purification of the Cys-free AS-A were performed according to the procedure as described in Chapter 2. The crystal of a binary complex of the Cys-free AS-A complexed with L-Asn were obtained as described in Chapter 2. The binary crystals were washed three times with a stock solution [50 mM HEPES (pH7.5), 56 % saturated ammonium sulfate, 10% glycerol, 15 mM $MgCl_2$, and 15 mM L-Asn. The crystal of a ternary complex of the Cys-free AS-A complexed with AMP and L-Asn were prepared by soaking the binary crystals for 10 days into the stock solution including AMP and L-Asn [50 mM HEPES (pH7.5), 56 % saturated ammonium sulfate, 10% glycerol, 15 mM $MgCl_2$, 50 mM AMP and 50mM L-Asn].

X-ray Diffraction Data Collection

The X-ray diffraction intensity data sets of the ternary complex crystals were collected with an R-AXIS IIc imaging plate mirror-mirror optics system equipped with 0.00015 inch filter mounted on a Rigaku RU-300 ($\lambda = 1.5418$Å) operated at 40 kV and 100 mA The intensity data were processed by using an R-AXIS IIc software (Sato *et al.*, 1992). The statistics of the data collection and the crystal parameters obtained are listed in Table 4-1.

Structure Determination and Refinement

The crystal structure of the binary complex including L-Asn was used for an initial model to refine the structure of the ternary complex including AMP and L-Asn. The refinement was performed with the program X-PLOR version 3.1 (Brünger *et al.*, 1987; Brünger, 1992b). At first the diffraction data of the range 10 - 2.5 Å resolution with $F >$

2σ (F) was refined by using simulated annealing and positional refinement protocols. The R-factor was fallen down from 0.35 to 0.19. At this stage $2F_o\text{-}F_c$ and $F_o\text{-}F_c$ maps showed the electron density of AMP and L-Asn. The AMP and L-Asn molecules were modeled by using the program TURBO-FRODO (Jones $et\ al.$, 1991). The resolution was then extended up to 2.2 Å, and simulated annealing refinement, positional refinement and individual B-factor refinement were carried out. Manual model re-building was carried out by picking of water molecules by using $2F_o\text{-}F_c$ and $F_o\text{-}F_c$ maps on TURBO-FRODO, and the models was refined by X-PLOR.

Manually model re-building with picking of water molecules using $2F_o\text{-}F_c$ and $F_o\text{-}F_c$ map on TURBO-FRODO and the position refinement of the model with X-PLOR were carried out alternatively. The water molecules were picked with the program WATER HUNTER (S. Sugio, unpublished). Statistics for the crystallographic refinement are summarized in Table 4-2.

Sequence Comparison of AS-As

Sequence comparison of AS-As was carried out by the program CLUSTAL V (Higgins $et\ al.$, 1992).

4 - 3. Results

Quality of the Ternary Complex Structure

The crystal structure of a ternary complex of the Cys-free AS-A with AMP and L-Asn was determined in order to identify the binding site of AMP. The X-ray diffraction data of the crystals of the ternary complex were observed as the unique 25184 reflections in the range of ∞ - 2.2 Å resolution [$I > 1\sigma$ (I)] with R_{merge} of 11.2 %. The crystallographic parameters and the statistics of the data collection of the ternary complex crystals were summarized in Table 4-1. The structure determination of the ternary complex was carried out by using the structure model of a binary complex of the Cys-free AS-A with L-Asn as a initial model. The structure of the ternary complex was refined by the program X-PLOR version 3.1 (Brünger $et\ al.$, 1987) to an R-factor of 18.7 % for 24815 reflections between 10 and 2.2 Å resolution [$F > 2\ \sigma(F)$]. The positions of AMP and L-Asn were assigned by using $2F_o\text{-}F_c$ and $F_o\text{-}F_c$ maps and then identified by the $2\ F_o\text{-}F_c$ and $F_o\text{-}F_c$ omitted maps. The final model includes 654 amino acids, 4 ligands and 209 water molecules. Summary of the refinement statistics is shown in Table 4-2. The distribution of torsion angles (Ramachandran plot) (Ramachandran $et\ al.$, 1974) of the ternary complex was calculated by the program PROCHECK (Laskowski, 1993) and is

shown in Figure 4-2. The maximum coordinate error of the ternary complex was calculated as 0.25 Å estimated by a Luzzati plot (Luzzati, 1952) as shown in Figure 4-3. The plot of the averaged temperature factor of the main chain atoms and the side chain atoms in the ternary complex is shown in Figure 4-4. The averaged temperature factor of protein region in the ternary complex were 9.9 Å^2.

Table 4-1. Summary of the crystallographic data and the data collection of the ternary complex crystals of the Cys-free Asparagine Synthetase with AMP and L-Asn.

Crystal system		monoclinic
Space group		$P2_1$
Cell constant	a (Å)	53.0
	b (Å)	126.1
	c (Å)	52.9
	β (degree)	105.6
Camera length (mm)		100.0
Spindle axis		+a*
Oscillation angle (degree / frame)		1.5
Exposing time (min. / frame)		10
No. of photos		130
Resolution (Å)		2.2
R_{merge} (%)[¶]		11.22
Accepted reflections ($I > 1\sigma\ (I)$)		71426
Unique reflections ($I > 1\sigma\ (I)$)		25184
Completeness (∞ - 2.2 Å) (%)		72.1
Completeness (2.3 - 2.2 Å) (%)		53.9
Temperature (°C)		20

$$^{\P}R_{merge} = \frac{\sum\sum\left|\langle I_{h,i}\rangle - I_{h,i}\right|}{\sum\sum I_{h,i}}$$

The ternary complex structure consisted of the dimer as observed for the binary complex structure. The main chain of the ternary complex is almost identical that of the binary complex. The root mean square difference between the ternary complex and the binary complex was calculated as 0.35 Å for α-carbons and 0.38 Å for main chain atoms. The observed hydrogen bonding interactions between subunits are summarized in Table 4-3-1. The α1 helix in the subunit A forms a hydrogen bonding with the β1 strand in the subunit B. The main chain amide nitrogen of Lys60 from the subunit A interacts with the main chain amide carbonyl of Pro101 from the subunit B. The subunit-subunit interaction by hydrogen bonding in the dimer of ternary complex is similar to that of the interaction in the dimer of binary complex. A number of hydrogen bonding interactions between subunits including through water molecules are observed in the ternary structure as shown in Table 4-3-2, while no hydrogen bonding through water molecules was observed for the subunit-subunit interaction in the binary structure.

Table 4-2. Refinement statistics of the ternary complex of the Cys-free Asparagine Synthetase with AMP and L-Asn.

Resolution(Å)	10.0-2.2
Reflections $(F>2\sigma(F))$	24815
No. of protein atoms	5118
No. of ligand atoms	64
No. of solvents	203
$R_{cryst}(\%)$	18.7
$R_{free}(\%)$	29.3
R.m.s. bond length (Å)	0.009
bond angle (degree)	1.24
dihedral (degree)	26.7
improper (degree)	2.22
Average B-factor of enzyme (Å^2)	9.9
ligand (Å^2)	15.8
solvent (Å^2)	15.8

$R_{cryst} = 100 \times \Sigma \, |F_o - F_c| / \Sigma \, |F_o|$
R_{free} was calculated using 10 % data chosen randomly and omitted from the refinement.
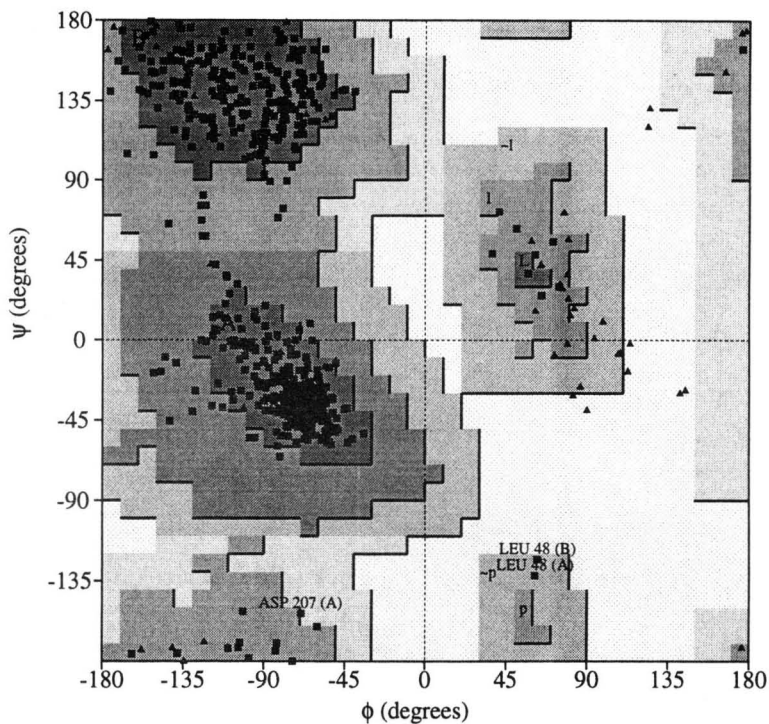
Figure 4-2. Ramachandran plot of the ternary complex of Asparagine Synthetase with AMP and L-Asn. The plot was produced with the program PROCHECK. Glycine residues are shown in triangles.
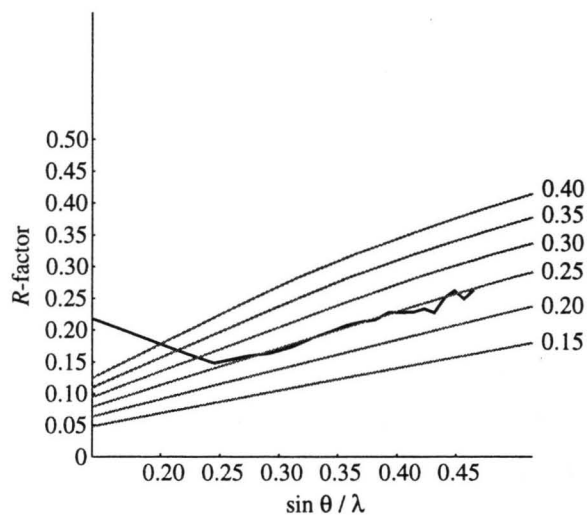

Figure 4-3. Luzzati plot for the refined structure of the ternary complex of Asparagine Synthetase with AMP and L-Asn. Gray lines are calculated Luzzati lines for coordinate errors. The maximum coordinate error of the binary complex was calculated as 0.25 Å.
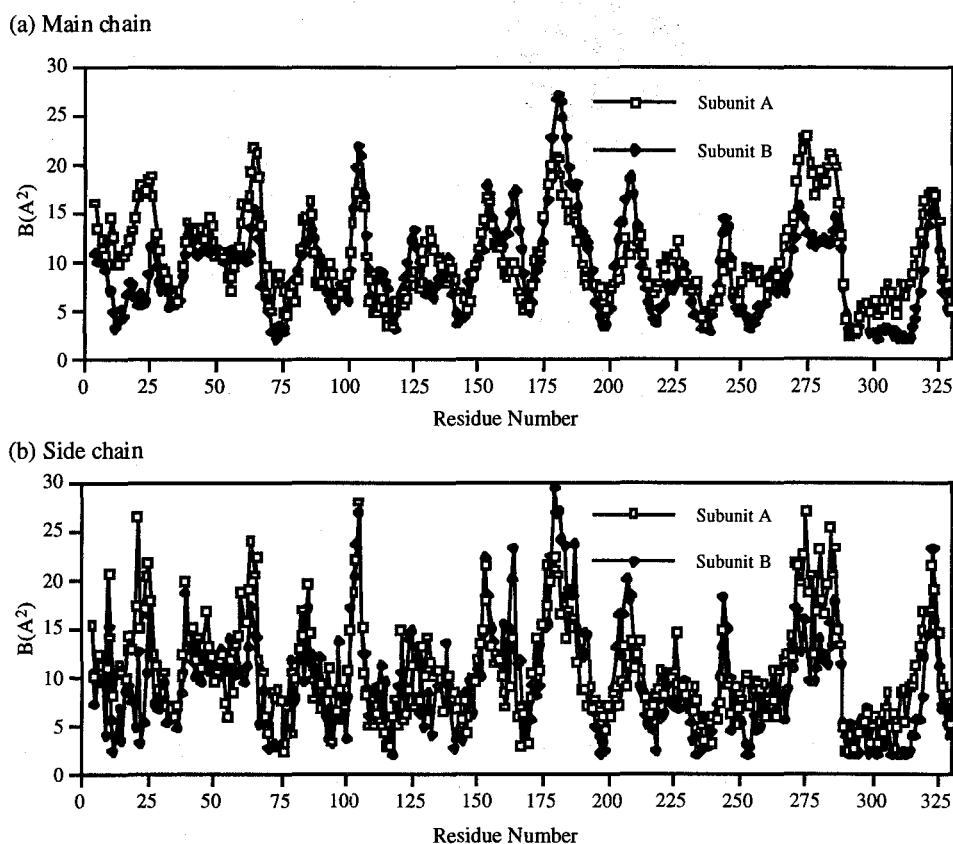
(a) Main chain

(b) Side chain

Figure 4-4. Plots of the temperature factor of the ternary complex of Asparagine Synthetase with AMP and L-Asn (a) Main chain (b) Side chain.

AMP and L-Asn Binding Site

The binding site of AMP of AS-A was found to be located on the central eight-stranded β-sheet as shown in Figure 4-5 and 4-6. Figure 4-7 shows the hydrogen-bonding network and the electrostatic interactions between the enzyme and the AMP. Adenine ring was located on the hydrophobic region formed by the side chain of Val114 and Arg299. The N1 atom of the adenine ring was in close proximity to the main chain amide nitrogen of Ser111. The N6 atom interacted with the main chain amide carbonyl of Leu109 and the side chain of Glu103. Ribose sit on the β-sheet β10 and β11. The 2'- and 3'- hydroxyl group of the ribose formed a polar interaction with the main chain amide nitrogen of Gly296 in the β11 and the main chain amide carbonyl of Ser250 in the β10, respectively. The α-phosphate oxygens are hydrogen-bonded to the side chain of Arg100.

The binding site of L-Asn is almost the same compared to the L-Asn binding site of the binary complex (Figure 4-5 and 4-6). As shown in Figure 4-6, the α-carboxyl

Table 4-3-1. Polar interactions between subunits.

Subunit A				Subunit B			Distance (Å)
Residue		Atom		Residue		Atom	
Q	9 A	OE1	-	Q	33 B	N	3.00
S	13 A	OG	-	E	31 B	OE2	3.22
E	31 A	OE2	-	S	13 B	OG	3.45
Q	33 A	N	-	Q	9 B	OE1	3.03
K	60 A	N	-	P	101 B	O	2.92
K	60 A	NZ	-	D	102 B	O	2.86
K	60 A	NZ	-	E	103 B	O	2.52
K	60 A	NZ	-	D	104 B	N	3.43
P	101 A	O	-	K	60 B	N	3.17

Table 4-3-2. Dimer interaction by hydrogen bonding through water molecule.

Water			Subunit or Water			Distance (Å)
H_2O	34	-	E	31 A	O	3.46
H_2O	34	-	Q	9 B	O	2.75
H_2O	47		Q	56 A	N	3.06
H_2O	47		Q	56 B	O	3.31
H_2O	137	-	A	315 A	O	2.64
H_2O	137	-	I	36 B	N	2.84
H_2O	137	-	L	37 B	N	2.97
H_2O	163	-	P	101 A	O	3.12
H_2O	163	-	E	103 A	O	2.81
H_2O	163	-	K	60 B	N	2.97
H_2O	163	-	A	61 B	N	2.83
H_2O	58	-	Q	9 A	O	3.11
H_2O	58	-	E	31 B	O	2.77
H_2O	58	-	H_2O 157		O	3.27
H_2O	157	-	S	13 A	OG	2.94
H_2O	157	-	Q	33 B	NE2	2.83
H_2O	102	-	K	58 A	N	2.86
H_2O	81	-	H_2O 102		O	2.80
H_2O	81	-	K	53 B	O	2.98

group of L-Asn interacted with the side chain of Lys77 and Arg255. The amino group of L-Asn is hydrogen-bonded to the main chain amide carbonyl of Ser251. The oxygen atom of the carbamoyl group of L-Asn formed a polar interaction with the side chain of Ser72 and Gln116, and the nitrogen atom of the L-Asn carbamoyl group interacts with the side chain of Asp46 and Tyr218.

Comparison of Catalytic Residues between AS-A and AspRS

AS-A and the catalytic domain of scAspRS were similar, and the common catalytic residues were conserved as described in Chapter 3. Then the positional differences of the catalytic residues in the ternary complex of AS-A with AMP and L-Asn and the ternary complex of scAspRS with ATP and tRNA^{Asp} (Cavarelli *et al.*, 1994) were compared by calculating the root mean square difference between the catalytic residues of both structures. Superposition of the positions of α-carbon, main chain and side chain gave the root mean square difference of 0.69 Å, 0.81 Å and 1.34 Å, respectively. As shown in Figure 4-8, the structural arrangement of these catalytic residues and AMP moiety in both enzymes was almost the same, indicating that most of the catalytic residues of AS-A and scAspRS were conserved. It is suggested that the manner of the catalytic residues are similar in each enzyme.
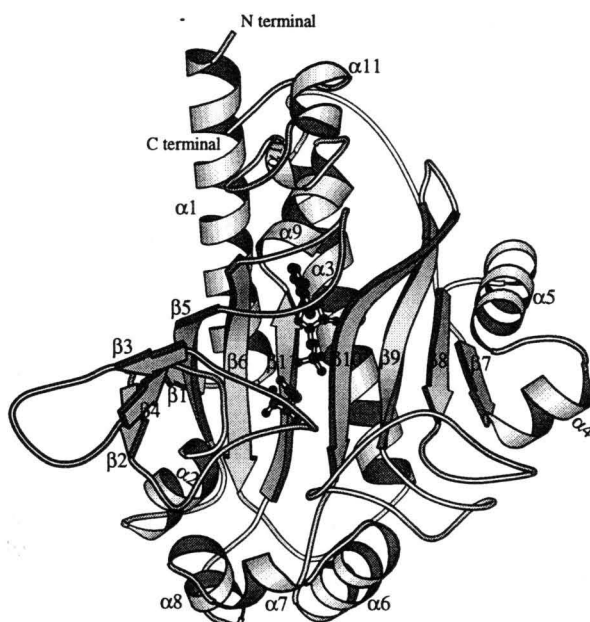

Figure 4-5. Ribbon diagram of a subunit structure of the ternary complex of Asparagine Synthetase with AMP and L-Asn. Bound AMP and L-Asn molecules are illustrated in ball-and-stick models. The ribbon drawing is generated by the program MOLSCRIPT.
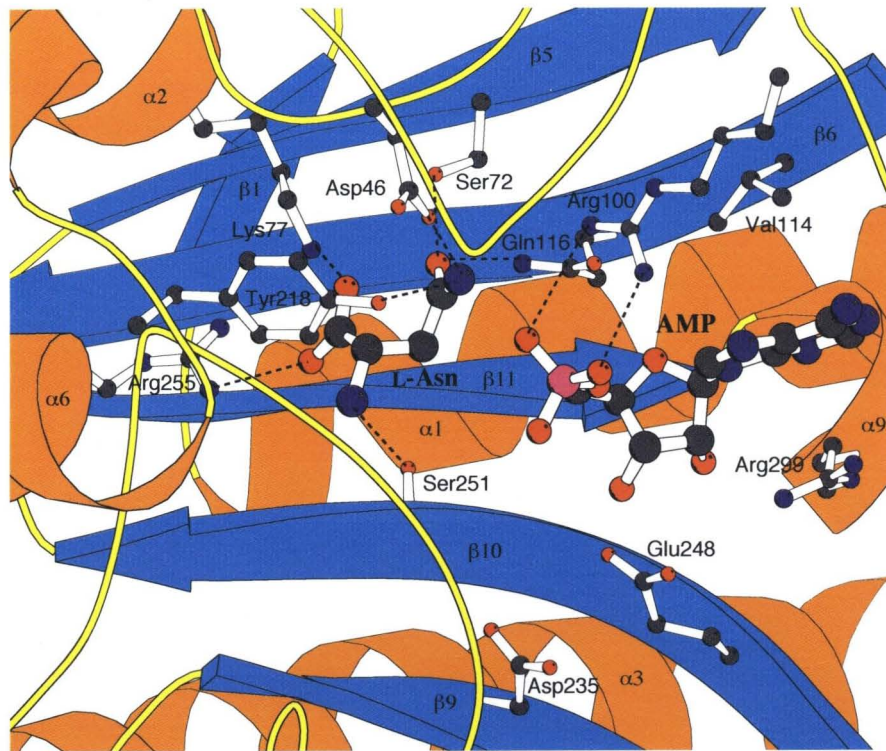
Figure 4-6. Schematic drawing of the catalytic region of Asparagine Synthetase complexed with AMP and L-Asn. AMP, L-Asn, the main chain carbonyl group of Ser251 and the side chain are illustrated by ball-and-stick models. Black balls show carbon atoms. Red and blue balls show oxygen and nitrogen atoms, respectively. Pink ball shows a phosphorus atom. Dashed lines show polar interactions.
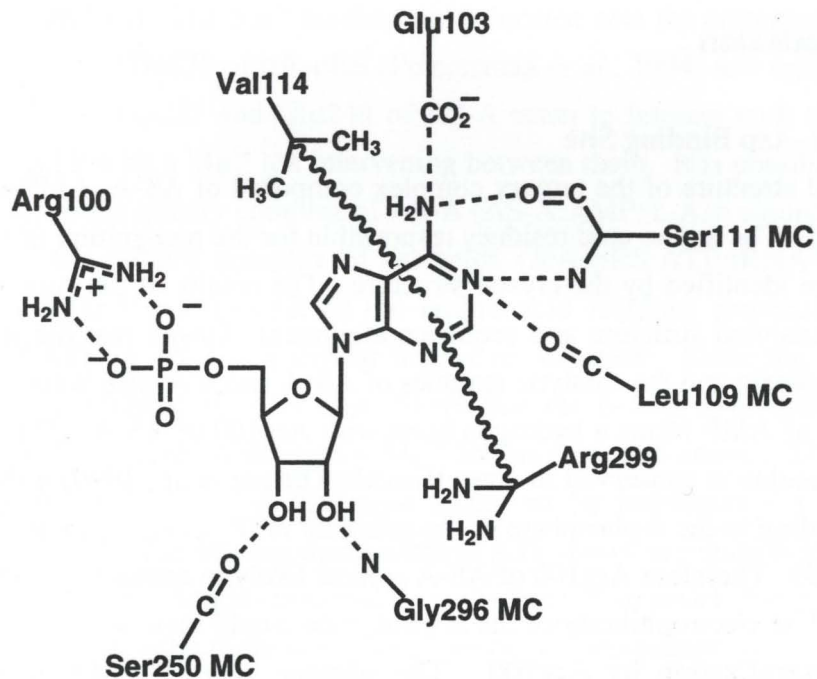

Figure 4-7. Schematic drawing of the interactions between AMP and AS-A. Dashed and waved lines correspond to hydrogen bonds and hydrophobic interactions, respectively.
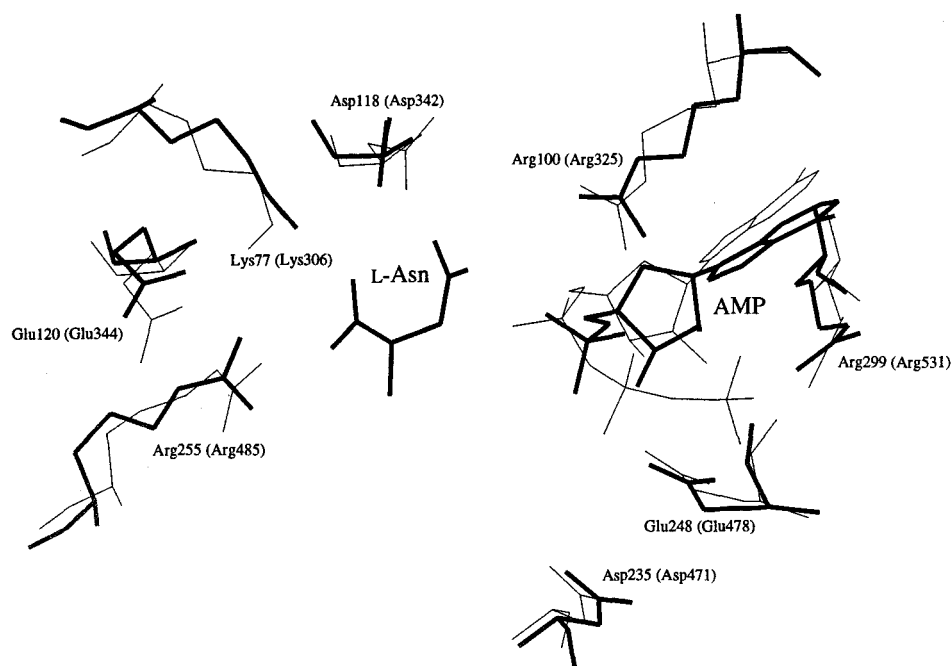
Figure 4-8. Superposition of the catalytic residues between of Asparagine Synthetase (bold line) and Aspartyl-tRNA Synthetase from *S. cerevisiae* (thin line). The residue number shows the sequence number of Asparagine Synthetase. The corresponding sequence number of Aspartyl-tRNA Synthetase shows in the parenthesis.

4 - 4. Discussion

ATP and L-Asp Binding Site

The crystal structure of the ternary complex composed of AS-A, AMP and L-Asn was determined. The amino acid residues responsible for the recognition of both AMP and L-Asn were identified by the crystal structure. The results of the superposition of the three dimensional structure and sequence alignment showed that the structure of the catalytic domain and the catalytic residues of AS-A and scAspRS were similar. The α-phosphate of AMP forms a hydrogen bond with Arg100 of AS-A. The corresponding arginine residue is conserved in class II aaRSs (Eriani *et al.*, 1990) and is responsible for the binding to the α-phosphate of the substrate ATP (Cavarelli *et al.*, 1994; Belrhali *et al.*, 1995). Therefore Arg100 of AS-A is most likely to interact with the α-phosphate of ATP. The electrophilicity of the α-phosphate would then be enhanced through the charge neutralization by Arg100. The adenine ring of AMP is located in the hydrophobic region formed by Val114 and Arg299 in AS-A. The valine residue is conserved in AS-As from *Escherichia coli, Haemophilus. influenzae* (Fleischmann *et*

al., 1995) and *Lactobacillus bulgaricus* (Kim *et al.*, 1996) as shown in sequence alignment (Figure 4-9), but is replaced by phenylalanine residue among all class II aaRSs (Eriani *et al.*, 1990). The difference of the corresponding residue of AS-A and aaRSs for the recognition of the adenine ring is most likely to reflect to the fact that the K_M for ATP of AS-A is about 10^2-fold that of aaRSs. It was evident that the position of Arg299 of AS-A structurally corresponds to the position of Arg531 in scAspRS by comparing the crystal structure of both enzymes as shown in Figure 4-8. The corresponding arginine residue is also an invariant residue among class II aaRSs (Eriani *et al.*, 1990). The arginine residue interacts not only with the adenine ring but also with the γ-phosphate of ATP in classII aaRS (Cavarelli *et al.*, 1994; Belrhali *et al.*, 1995). Therefore Arg299 of AS-A is also expected to be hydrogen-bonded to the γ-phosphate of ATP. As shown in Figure 4-8, the positions of Asp235 and Glu248 of AS-A correspond to that of Asp471 and Glu478 of scAspRS, respectively, by comparing the crystal structure of both enzymes. These acidic residues of scAspRS are conserved in all class II aaRSs for positioning the β- and γ- phosphates of ATP through a Mg^{2+} ion (Cavarelli *et al.*, 1994). The Mg^{2+} ion does not detected in the ternary complex structure of AS-A. The Sm^{3+} ion binds to Asp235 and Glu248 in the AS-A crystals containing Sm^{3+} ion which were prepared to calculate the phase by using the MIR method. The Sm^{3+} binding site is compatible to the Mg^{2+} binding site of scAspRS. The Mg^{2+} binding site of ttAspRS was also determined by using the ttAspRS crystals containing the Sm^{3+} ion. The Sm^{3+} binding site is located near the corresponding acidic residues Asp469 and Glu476 of ttAspRS (Poterszman *et al.*, 1994) and agrees with that of scAspRS. Thus Asp235 and Glu248 of AS-A seem to interact with the β- and γ-phosphates of ATP with a Mg^{2+} ion intervening between them. It is possible to replace the AMP model of the ternary complex of AS-A (AS-A:AMP: L-Asn complex) with the ATP model of the ternary complex of scAspRS (scAspRS:ATP:tRNA^{Asp} complex) because the role and arrangement of the amino acid residues responsible for the recognition of ATP in AS-A are similar to that of scAspRS. Since the ATP model forms the bent conformation, it is most likely that the β- and γ- phosphate bind to Asp235 and Glu248 of AS-A through a Mg^{2+} ion as expected above. Thus Asp235, Glu248, Arg299 and Mg^{2+} ion are most likely to be important for the correct conformation of ATP. The binding mechanism of ATP shows in Figure 4-10.

The position of L-Asp is estimated by replacing L-Asn with L-Asp in the ternary complex structure, although there is no direct structural information of the substrate of L-Asp. The manner of binding L-Asp to AS-A is shown in Figure 4-10. Lys77 and Arg255 in AS-A are hydrogen-bonded to one of the two oxygen atoms of the α-

```
                1        10        20        30        40        50
E.coli   MKT-----AY-----IAKQRQISFVKSHFSRQLEERLGLIEVQAPILSRVGDGTQDNLSGCEKAVQVKV
H.infl   MKK-----TF-----ILQQQEISFVKNTFTQNLIEQLGIIEVQGPILSQVGNGMQDNLSGIEKAVQVNV
L.bulg   MAKLVIPSDYDPKMTIAKRKRQSATSGKPSSEFGTAMNLERISAPMFVKKSSGLNDNLSGWEKPVSFTL
         *       .      *   ...  *      . ...  .. . . .*.. . . * .***** **.*    .


                60       70        80        90       100       110       120
E.coli   KALPDAQFEVVHSLAKWKRQTLGQHDFSAGEGLYTHMKALRPDEDRLSPLHSVYVDQWDWERVMGDGER
H.infl   KCIPNAVFEVVHSLAKWKRHTLARFNFKEDEGLFVHMKALRPDEDSLDPTHSVYVDQWDWEKVIPEGRR
L.bulg   HDGNEGELQIVHSLAKWKRWALKHYGFSHGEGLFTNMNAIRKDEEVLDNLHSVYVDQWDWEKVIDKSER
         ..  ...*********  .*  .  * .***. .*.*.* **. *    **********.*.  . *


               130      140       150       160       170       180       190
E.coli   QFSTLKSTVEAIWAGIKATEAAVSEEFGLAPF-LPDQIHFVHSQELLSRYPDLDAKGRERAIAKDLGAV
H.infl   NFAYLKETVNSIYRAIRLTELAVEARFDIPSI-LPKQITFVHSEDLVKRYPDLSSKERENAICKEYGAV
L.bulg   TEATLRQTVQRIFETIKGMEYHVRALYPQAAYHLPEEISFVTSEELEARWPSLTPSEREDKICQEKGAV
         . *. **. *   *. * *  .   ..  ** .* ** *..*  * * *  .  **  *  .. ***


               200      210       220       230       240       250       260
E.coli   FLVGIGGKLS-DGHRHDVRAPDYDDWSTPSELGHAGLNGDILVWNPVLEDAFELSSMGIRVDADTLKHQ
H.infl   FLIGIGGKLS-DGKPHDGRAPDYDDWTTESENGYKGLNGDILVWNDQLGKAFELSSMGIRVDESALRLQ
L.bulg   FLEHIGGALPLSKKPHDLRAPDYDDWT---------LNGDLLFWYEPLQRAFEVSSMSIRVDEDRLQEQ
         **  *** *.     ** *******.      ****.* *   *  ***.***.****    *. *


               270      280       290       300       310       320       330
E.coli   LALTGDEDRLELEWHQALLRGEMPQTIGGGIGQSRLTMLLLQLPHIGQVQCGVWPAAVRESVPS----LL
H.infl   VGLTGDEDHLKMDWHQDLLNGKLPLTIGGGIGQSRLAMLLLRKKHIGEVQSSVWPKEMLEEFSN----IL
L.bulg   LKLAGAEDRLDLPFHQALLKGDLPYSIGGGIGQSRLCMLLLQGPH-GEVQASIWPDEIVEKCQAAKIQLL
         i . *.* **.* .  ** ** * .* .********* ****. * *.** ..**  . *       .*
```

Figure 4-9. Sequence comparison of Asparagine Synthetases from *Escherichia coli* (E. coli), *Haemophilus. influenzae* (H. infl) and *Lactobacillus bulgaricus* (L. bulg). The number is the sequence number of the enzyme from *Escherichia coli*. Asterisks (*) are conserved residues in all AS-As. Dots (.) are similar characteristic residues in all AS-As.

carboxyl group of L-Asp. The side chains of these residues are positioned by the hydrogen bond interaction with the side chain of Glu120 so as to interact with the α-carboxyl group of L-Asp. A similar hydrogen bonding network involving Lys-Glu-Arg was found in AspRS at the binding site of the β-carboxyl group of L-Asp substrate and these residues were conserved in AspRSs (Cavarelli *et al.*, 1994; Poterszman *et al.*, 1994). These three residues are also conserved in AS-As as shown in Figure 4-9. Because the recognition mechanism of the carboxyl group is similar, and the catalytic residues are conserved in both enzymes, the Lys-Glu-Arg hydrogen bonding network might be responsible for the correct positioning of the substrate carboxyl group for both enzymes. The nitrogen atom of the carbamoyl group of Gln116 in AS-A forms a hydrogen bond with the β-carboxyl group of L-Asp. The side chain of Gln116 is positioned by the hydrogen bond interaction with the carboxyl group of Asp118 so as to

interact with the β-carboxyl group of L-Asp. Ser251 and Asp219 in AS-A interact with the amino group of the L-Asp: the main chain carbonyl group of Ser251 is hydrogen-bonded to the amino group of the L-Asp, and the carboxyl group of Asp219 also interacts with the same amino group through a water molecule. Ser251 and Asp219 are key residues of the correct conformation of the L-Asp binding in AS-A. The β-carboxyl group of the L-Asp locates on the opposing side of the α-phosphorus relative to the pyrophosphate leaving group as shown in Figure 4-10. The α-phosphate of ATP is exposed to L-Asp so as to subject the nucleophilic attack of the β-carboxyl group of L-Asp.
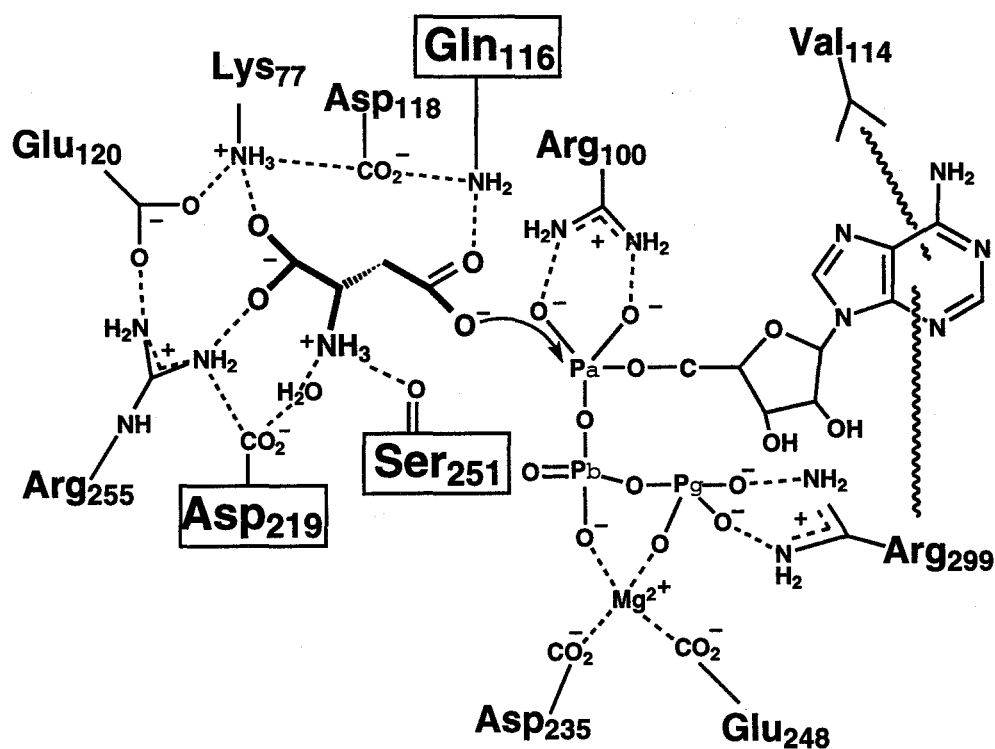
Figure 4-10. Schematic drawing for the proposed the binding mechanism of the substrates; L-Asp and ATP of Asparagine Synthetase. The boxed amino acids do not have residues whose role does not exist in Aspartyl-tRNA Synthetase from *S. cerevisiae*.

Reaction Mechanism for β-Aspartyl-AMP Formation by AS-A

AS-A and aaRSs are believed to catalyze by two-step reaction mechanism (Meister, 1974; Schimmel, 1987), especially the first reaction step is common in the point of view the formation of enzyme-bound aminoacyl-adenylate intermediate. The amino acylation reaction progress by the nucleophilic attack by the carboxyl group of an amino acid in aaRSs (Knowles, 1980). It is suggested that aaRSs catalyze the formation of the aminoacyl-adenylate by an in-line mechanism (Langdon *et al.*, 1979; Harnett *et al.*, 1985). In addition the mechanism of aaRSs is supported by the structural studies by AspRS, SerRS and GlnRS (Perona *et al.*, 1993; Cavarelli *et al.*, 1994; Belrhali *et al.*, 1995). In the in-line mechanism, the entering and leaving groups which are amino acid and pyrophosphate, respectively, are an opposite sides of α-phosphorus atom of ATP, forming a straight line with the α-phosphorus. This reaction passes through a pentavalent intermediate, in which three of the oxygen atoms lie in a plane with the α-phosphorus atom in aaRSs. The mechanism results in stereochemical inversion of the configuration around the α-phosphorus.

The recognition mechanism of the substrates; ATP and L-Asp of AS-A are shown in Figure 4-10. The conformation and position of the substrates are similar to that of scAspRS. Especially the binding mechanism of ATP is almost the same in the both enzymes. The proposed L-Asp binding site of AS-A positions the β-carboxyl group of this ligand on the opposing side of the α-phosphorus relative to the pyrophosphate leaving group. The straight conformation of the β-carboxyl group, the α-phosphorus and the pyrophosphate is most likely to support the in-line mechanism for the formation of β-aspartyl-adenylate by AS-A. Arg100 of AS-A plays a key role in positioning the α-phosphate and in charge neutralization. The arginine residue interacts with α-phosphate of ATP and is conserved in AS-As as shown in Figure 4-9. The corresponding invariant arginine residue conserved in all aaRSs also binds to the α-phosphate of ATP. In addition it was reported that the arginine residue involved in the stabilization of the trigonal bypyramidal transition state at α-phosphate in AspRS and SerRS (Cavarelli *et al.*, 1994; Belrhali *et al.*, 1995). The amino acylation reaction of AS-A also might be pass through the trigonal bipyramidal transition state because the arrangement and binding residues of the substrates; L-Asp and ATP are very similar. Thus Arg100 of AS-A is also likely to stable the transition state. Arg299 of AS-A binds to the γ-phosphate of ATP so as to form the bent conformation. The arginine residue and the Mg^{2+} ion which binds to β- and γ- phosphate, stabilize the bent conformation and help to polarize the target α-phosphate group for nucleophilic attack. Because the

position of the β-carboxyl group of the substrate L-Asp is close to the α-phosphate of ATP which is negatively charged by the arginine residues and Mg^{2+} ion, the β-carboxyl group of L-Asp attacks to the α-phosphate of ATP from the opposite side of the pyrophosphate so as to form a trigonal bypyramidal transition state at the α-phosphorus atom. The pyrophosphate leaving group is neutralized and stabilized by the Mg^{2+} ion. Then AS-A releases the pyrophosphate and forms the enzyme-bound β-aspartyl-adenylate. Therefore the formation of the β-aspartyl-adenylate is most likely to attended with the stereochemical inversion of configuration of α-phosphorus atom of ATP in AS-A as observed in aaRSs.

CHAPTER 5

General Conclusion

The author has crystallized Asparagine Synthetase from *Escherichia coli* K-12 and has determined two types (AS-A:L-Asn complex and AS-A:AMP:L-Asn complex) of the three dimensional structure of AS-A by using the X-ray diffraction analysis in order to understand the structural basis for the catalytic functions.

The crystals of AS-A complexed with L-Asn could be obtained by using Cys-free (C51A/C315A) mutant AS-A because the wild AS-A only gave the needle crystals which were not suitable for X-ray diffraction analysis. The Cys-free AS-A crystals were obtained by the sitting drop vapour diffusion method at 20 °C using ammonium sulfate as precipitant. The quality of the crystals was improved by the addition of L-Asn. The AS-A crystals belong to the space group of $P 2_1$ with the cell dimensions of $a = 52.9$ Å, $b = 126.2$ Å, $c = 52.8$ Å and $\beta = 105.3°$.

The three dimensional structure of the binary complex of AS-A with L-Asn has been determined at 2.5 Å resolution by the multiple isomorphous replacement method using two types of derivative crystals containing $Sm_2(SO_4)_3$ or $K_2Pt(CN)_4$. The R-factor became 15.4 % for 17241 reflections in the range of 10 - 2.5 Å resolution $[F > 2\sigma(F)]$. The overall structure is a homodimer, and the subunit structure consists of one domain composed of eleven α-helices and eleven β-strands. The characteristic fold of AS-A is six stranded antiparallel β-sheet flanked with two long α-helices which fold has ever been only detected in the catalytic domain of aaRSs. The fold of AS-A is especially similar to the catalytic domain of scAspRS, although the amino acid sequence of AS-A was quite different from that of scAspRS. Furthermore, it was found that a lot of catalytically important residues were conserved in both enzymes by the superposition based on the three dimensional structure. As the results, it is suggested that the evolutional relationship is the divergent evolution because the three dimensional structure and reaction mechanism are similar in both enzymes.

The author, furthermore, has determined the ternary complex of AS-A with AMP and L-Asn at 2.2 Å resolution in order to explicate the recognition mechanism for the substrates; ATP and L-Asp and the reaction mechanism for the formation of β-aspartyl adenylate intermediate. The R-factor became 18.7 % for 24815 reflections in the range of 10 and 2.2 Å resolution $[F > 2 \sigma(F)]$. The binding sites of AMP and L-Asn were located on the antiparallel β-sheet as well as scAspRS. The binding mechanism of AMP moiety was almost the same in both enzymes. In addition, the superposition of

the amino acid residues around AMP moiety in both enzymes revealed the conservation of amino acid residues responsible for the binding of β- and γ- phosphate of ATP. Thus it was found that Arg100 and Arg299 are most important residues in the recognition of α- and γ- phosphate, respectively. In addition Asp235 and Glu248 were involved in the recognition of β- and γ- phosphate through Mg^{2+} ion. The network of Lys-Glu-Arg responsible for the recognition of the carboxyl group of the substrate L-Asp conserved in AS-A and AspRS, however, the α- and β- carboxyl group of L-Asp interacted with the network in AS-A and AspRS, respectively, namely the binding mechanism of the substrate is different in both enzymes. Asp219 of AS-A is involved in the recognition of the amino group of the substrate L-Asp, however, Asp342 of scAspRS responsible for the recognition of the amino group of L-Asp is located on the opposite side for the residue of AS-A. Gln116 of AS-A interacted with the β-carboxyl group of the substrate L-Asp which was closely located on the α-phosphate of ATP. Arg100 of AS-A plays a key role in positioning of the α-phosphate and in charge neutralization. In addition, Arg299 of AS-A is involved in the γ-phosphate of ATP so that the pyrophosphate of ATP locates on the opposite side of the β-carboxyl group. Thus the β-carboxyl group attacks to the α-phosphate from the opposite side of pyrophosphate, consequently the amino acylation reaction pass through the in-line mechanism and results in the stereochemical inversion of the configuration around the α-phosphorus. Therefore AS-A forms the enzyme-bound β-aspartyl AMP and releases the pyrophosphate which is stabilized by the bound Mg^{2+} ion. The amino acylation reaction might be pass through the trigonal bipyramidal transition state at α-phosphate of ATP. Arg100 is most likely to stable to the transition state.

Appendix

(1) **doall.sh**: the shell script consists of six following shell scripts.

```
# COMMAND PROCEDURE TO CARRY OUT THE ENTIRE CYCLING PROCESS FOR PHASING
# DATA BY SOLVENT LEVELLING
# COMPUTE THE FIRST SOLVENT MASK
sh mask1.sh
#
# COMPUTE 4 CYCLES OF SOLVENT LEVELLING (USING FIRST MASK)
sh cycle4.sh
#
# COMPUTE THE SECOND SOLVENT MASK
sh mask2.sh
#
# COMPUTE 4 CYCLES OF SOLVENT LEVELLING (USING SECOND MASK)
sh cycle8.sh
#
# COMPUTE THE THIRD SOLVENT MASK
sh mask3.sh
#
# COMPUTE 8 CYCLES OF SOLVENT LEVELLING (USING THE THIRD MASK)
sh cycle16.sh
# THATS ALL
```

mask1.sh

```
# COMPUTE ORIGINAL ELECTRON DENSITY MAP
ln phasit.31 four.ref
fsfour < fft.d > mask1.1
mv four.map orig.map
rm four.ref
ln orig.map four.map
#
# REMOVE HEAVY ATOM PEAKS FROM MAP
rmheavy < rmhv.d >> mask1.1
mv nohv.map four.map
#
# INVERT MAP AFTER TRUNCATING DENSITY < 0
mapinv < minv1.d >> mask1.1
rm four.map
#
# MULTIPLY FOURIER COEFICIENTS BY TRANSFORM OF WEIGHTING FUNCTION
bndry < bnd0.d >> mask1.1
rm minv.ref
#
# COMPUTE "SMEARED" MAP FROM MODIFIED COEFICIENTS
fsfour < fft.d >> mask1.1
rm four.ref
#
# DETERMINE PROTEIN-SOLVENT BOUNDARY MASK FROM "SMEARED" MAP
bndry < bnd1.d >> mask1.1
mv mask.map mask1.14
rm four.map
# THATS ALL
```

mask2.sh

```
# COMPUTE ELECTRON DENSITY MAP
ln phi4cy.31 four.ref
```

```
fsfour < fft.d > mask2.1
rm four.ref
#
# REMOVE HEAVY ATOM PEAKS FROM MAP
rmheavy < rmhv.d >> mask2.1
mv nohv.map four.map
#
# INVERT MAP AFTER TRUNCATING DENSITY < 0
mapinv < minv1.d >> mask2.1
rm four.map
#
# MULTIPLY FOURIER COEFICIENTS BY TRANSFORM OF WEIGHTING FUNCTION
bndry < bnd0.d >> mask2.1
rm minv.ref
#
# COMPUTE "SMEARED" MAP FROM MODIFIED COEFICIENTS
fsfour < fft.d >> mask2.1
rm four.ref
#
# DETERMINE PROTEIN-SOLVENT BOUNDARY MASK FROM "SMEARED" MAP
bndry < bnd1.d >> mask2.1
mv mask.map mask2.14
rm four.map
# THATS ALL
```

mask3.sh

```
# COMPUTE ELECTRON DENSITY MAP
ln phi8cy.31 four.ref
fsfour < fft.d > mask3.1
rm four.ref
#
# REMOVE HEAVY ATOM PEAKS FROM MAP
rmheavy < rmhv.d >> mask3.1
mv nohv.map four.map
#
# INVERT MAP AFTER TRUNCATING DENSITY < 0
mapinv < minv1.d >> mask3.1
rm four.map
#
# MULTIPLY FOURIER COEFICIENTS BY TRANSFORM OF WEIGHTING FUNCTION
bndry < bnd0.d >> mask3.1
rm minv.ref
#
# COMPUTE "SMEARED" MAP FROM MODIFIED COEFICIENTS
fsfour < fft.d >> mask3.1
rm four.ref
#
# DETERMINE PROTEIN-SOLVENT BOUNDARY MASK FROM "SMEARED" MAP
bndry < bnd1.d >> mask3.1
mv mask.map mask3.14
rm four.map
# THATS ALL
```

cycle4.sh

```
# MODIFY ELECTRON DENSITY MAP ACCORDING TO MASK1
# use .06 for 3A data and .086 for 3.5 and .112 for 4.A
mv orig.map four.map
ln mask1.14 mask.map
bndry < bnd2.d > cycle4.1
```

```
rm four.map mask.map
#
# INVERT MODIFIED MAP TO OBTAIN STRUCTURE FACTORS
mapinv < minv2.d >> cycle4.1
rm mod.map
#
# COMBINE PRIOR PHASE INFORMATION WITH THAT FROM MAP INVERSION
bndry < bnd3.d >> cycle4.1
#
# PERFORM 3 MORE CYCLES OF REFINEMENT
for cycle
in 1 2 3
do
#
# COMPUTE ELECTRON DENSITY MAP FROM COMBINED PHASE INFORMATION
rm minv.ref
mv newphi.ref four.ref
fsfour < fft.d >> cycle4.1
rm four.ref
#
# MODIFY ELECTRON DENSITY MAP ACCORDING TO MASK
ln mask1.14 mask.map
# use .06 for 3A,.086 for 3.5 and .112 for 4A
bndry < bnd2.d >> cycle4.1
rm four.map mask.map
#
# INVERT MODIFIED MAP TO OBTAIN STRUCTURE FACTORS
mapinv < minv2.d >> cycle4.1
rm mod.map
#
# COMBINE PRIOR PHASE INFORMATION WITH THAT FROM MAP INVERSION
bndry < bnd3.d >> cycle4.1
done
mv newphi.ref phi4cy.31
mv minv.ref allcoef.31
# THATS ALL
```

cycle8.sh

```
# START OVER USING NEW MASK
cp phasit.31 newphi.ref
ln phasit.31 minv.ref
#
# PERFORM 4 CYCLES OF REFINEMENT, USING SECOND MASK
for cycle
in 1 2 3 4
do
#
# COMPUTE ELECTRON DENSITY MAP FROM COMBINED PHASE INFORMATION
rm minv.ref
mv newphi.ref four.ref
fsfour < fft.d > cycle8.1
rm four.ref
#
# MODIFY ELECTRON DENSITY MAP ACCORDING TO MASK
ln mask2.14 mask.map
# use .06 for 3A,.086 for 3.5 and .112 for 4A
bndry < bnd2.d >> cycle8.1
rm four.map mask.map
#
```

```
# INVERT MODIFIED MAP TO OBTAIN STRUCTURE FACTORS
mapinv < minv2.d >> cycle8.1
rm mod.map
#
# COMBINE PRIOR PHASE INFORMATION WITH THAT FROM MAP INVERSION
bndry < bnd3.d >> cycle8.1
done
mv newphi.ref phi8cy.31
mv minv.ref allcoef.31
# THATS ALL
```

cycle16.sh

```
# START OVER USING NEW MASK
cp phasit.31 newphi.ref
ln phasit.31 minv.ref
#
# PERFORM 8 CYCLES OF REFINEMENT, USING THIRD MASK
for cycle
in 1 2 3 4 5 6 7 8
do
#
# COMPUTE ELECTRON DENSITY MAP FROM COMBINED PHASE INFORMATION
rm minv.ref
mv newphi.ref four.ref
fsfour < fft.d > cycle16.1
rm four.ref
#
# MODIFY ELECTRON DENSITY MAP ACCORDING TO MASK
ln mask3.14 mask.map
# use .06 for 3A,.086 for 3.5 and .112 for 4A
bndry < bnd2.d >> cycle16.1
rm four.map mask.map
#
# INVERT MODIFIED MAP TO OBTAIN STRUCTURE FACTORS
mapinv < minv2.d >> cycle16.1
rm mod.map
#
# COMBINE PRIOR PHASE INFORMATION WITH THAT FROM MAP INVERSION
bndry < bnd3.d >> cycle16.1
done
mv newphi.ref phi16cy.31
mv minv.ref allcoef.31
# THATS ALL
```

(2) **extndavg.sh**

```
# MODIFIED TO INCLUDE NONCRYSTALLOGRAPHIC SYMMETRY AVERAGING
# RESUME WHERE WE LEFT OFF AFTER FIRST 16 CYCLES
cp phi16cy.31 newphi.ref
ln phasit.31 minv.ref
#
# PERFORM 16 CYCLES OF PHASE EXTENSION/AVERAGING, USING THIRD MASK
for cycle
in 1 2 3 4 5 6 7 8 9 10 11 12 13 14 15 16
do
#
# COMPUTE ELECTRON DENSITY MAP FROM COMBINED PHASE INFORMATION
rm minv.ref
```

Appendix

```
mv newphi.ref four.ref
fsfour < fft.d >> extndavg.l
rm four.ref
#
# EXTRACT REGION FROM MAP APPROPRIATE FOR AVERAGING
extrmap < extrmap.d >> extndavg.l
#
# AVERAGE THE ELECTRON DENSITY, WITHIN THE MOLECULAR ENVELOPE
mapavg < mapavg.d >> extndavg.l
rm asu.map
#
# REBUILD THE COMPLETE UNIT CELL
bldcel < bldcel.d >> extndavg.l
rm four.map asu.avg
mv avgcell.map four.map
#
# MODIFY AVERAGED ELECTRON DENSITY MAP ACCORDING TO MASK
ln mask3.14 mask.map
# use .06 for 3A,.086 for 3.5 and .112 for 4A
bndry < bnd2.d >> extndavg.l
rm four.map mask.map
#
# INVERT MODIFIED MAP TO OBTAIN STRUCTURE FACTORS
mapinv < minv2.d >> extndavg.l
rm mod.map
#
# COMBINE PRIOR PHASE INFORMATION WITH THAT FROM MAP INVERSION
# AND EXTEND PHASING TO ADDITIONAL AMPLITUDES
bndry < extnd.d >> extndavg.l
done
mv newphi.ref phiextndavg.31
mv minv.ref allcoef.31
# THATS ALL
```

Acknowledgments

References

Andrulis, I. L., Chen, J. and Ray, P. N. (1987). *Mol. Cell. Biol.* **7**, 2435-2443.

Babbit, P. C., Mrachko, G. T., Hasson, M. S., Huisman, G. W., Kolter, R., Ringe, D., Petsko, G. A., Kenyon, G. L. and Gerlt, J. A. (1995). *Science* **267**, 1159-1161.

Belrhali, H., Yaremchuk, A., Tukalo, M., Berthet-Colominas, C., Rasmussen, B., Bösecke, P., Diat, O. and Cusack, S. (1995). *Structure* **3**, 341-352.

Bijvoet, J. M. (1954). *Nature* **173**, 888-891.

Bricogne, G. (1976). *Acta Crystallogr.* **A32**, 832-847.

Brünger, A. T. (1992a). *Nature* **355**, 472-475.

Brünger, A. T. (1992b). *X-PLOR version 3.1: A system for x-ray crystallographiy and NMR* New Heaven: Yale University press.

Brünger, A. T., Krukowski, A. and Erickson, J. (1990). *Acta Cryst.* **A46**, 585-593.

Brünger, A. T., Kuriyan, J. and Karplus, M. (1987). *Science* **235**, 458-460.

Cavarelli, J., Eriani, G., Rees, B., Ruff, M., Boeglin, M., Mitschler, A., Thierry, J.-C. and Moras, D. (1994). *EMBO J.* **13**, 327-337.

Cedar, H. and Schwartz, J. H. (1969a). *J. Biol. Chem.* **244**, 4112-4121.

Cedar, H. and Schwartz, J. H. (1969b). *J. Biol. Chem.* **244**, 4122-4127.

Collaborative computational project, N. (1994). *Acta Cryst.* **D50**, 760-763.

Cusack, S. (1995). *Nature Struct. Biol.* **2**, 824-831.

Davis, B. J. (1964). *Ann. N. Y. Acad. Sci.* **121**, 404-427.

Engh, R. A. and Huber, R. (1991). *Acta Cryst.* **A47**, 392-400.

Eriani, G., Cavarelli, J., Martin, F., Dirheimer, G., Moras, D. and Gangloff, J. (1993). *Proc. Natl. Acad. Sci.* **90**, 10816-10820.

Eriani, G., Deralue, M., Poch, O., Gangloff, J. and Moras, D. (1990). *Nature* **347**, 203-206.

Ferré-D'Amoré, A. R. and Burley, S. K. (1994a). *Structure* **2**, 357-359.

Ferré-D'Amoré, A. R., Pognec, P. and Burley, S. K. (1994b). *EMBO J.* **13**, 180-189.

Fleischmann, R. D., Adams, M. D., White, O., Clayton, R. A., Kirkness, E. F., Kerlavage, A. R., Bult, C. J., Tomb, J.-F., Dougherty, B. A., Merrick, J. M., McKenny, K., Sutton, G., FitzHugh, W., Fields, C., Gocayne, J. D., Scott, J., Shirley, R., Liu, L.-I., Glodek, A., Kelley, J. M., Weidman, J. F., Phillips, C. A., Spriggs, T., Hedblom, E., Cotton, M. D., Utterback, T. R., Hanna, M. C., Nguyen, D. T., Saudek, D. M., Brandon, R. C., Fine, L. D., Fitchman, J. L., Fuhrmann, J. L., Geoghagen, N. S. M., Gnehm, C. L., McDonald, L. A., Small,

K. V., Fraser, C. M., Smith, H. O. and Venter, J. C. (1995). *Science* **269**, 496-512.

Furey, W. and Swaminathan, S. (1996). *Methods in Enzymol.* in press. Orlando, FL: Academic Press.

Gantt, J. S. and Arfin, S. M. (1981). *J. Biol. Chem.* **256**, 7311-7315.

Gatti, D. L. and Tzagoloff, A. (1991). *J. Mol. Biol.* **218**, 557-568.

Green, D. W., Ingram, V. M. and Perutz, M. F. (1954). *Proc. R. Soc. London* **A225**, 287-307.

Harnett, S. P., Lowe, G. and Tansley, G. (1985). *Biochemistry* **24**, 2908-2915.

Higgins, D. G., Bleasby, A. J. and Fuchs, R. (1992). *CABIOS* **8**, 189-191.

Hinchman, S. K., Henikoff, S. and Schuster, S. M. (1992). *J. Biol. Chem.* **267**, 144-149.

Hongo, S. and Sato, T. (1981). *Anal. Biochem.* **114**, 163-166.

Hongo, S. and Sato, T. (1985). *Arch. Biochem. Biophys.* **238**, 410-417.

Humbert, R. and Simoni, R. D. (1980). *J. Bacteriol.* **142**, 212-220.

Jones, T. A., Zou, J.-Y., Cowan, J. W. and Kjelgaard, M. (1991). *Acta Crystallogr.* **A47**,

Kim, S. I., Germond, J.-E., Pridmore, D. and Söll, D. (1996). *J. Bacteriol.* **178**, 2459-2461.

Kirkpatrick, S., Gelatt, C. D. J. and Vecchi, M. P. (1983). *Science* **220**, 671-680.

Knowles, J. R. (1980). *Ann. Rev. Biochem.* **49**, 877-919

Kunkel, T. A. (1985). *Proc. Natl. Acad. Sci. USA* **82**, 488-492. Orlando, FL: Academic Press.

Kunkel, T. A., Roberts, J. D. and Zakour, R. A. (1987). *Methods in Enzymol.* **154**, 367-382.

Laemmli, U. K. (1970). *Nature* **227**, 680-685.

Langdon, S. P. and Lowe, G. (1979). *Nature* **281**, 320-321.

Laskowski, R. A. (1993). *J. Appl. Cryst.* **26**, 283-291.

Leslie, A. G. W. (1987). *Acta Crystallogr.* **A43**, 134-136.

Logan, D. T., Mazauric, M.-H., Kern, D. and Moras, D. (1995). *EMBO J.* **14**, 4156-4167.

Lorber, B. and Giegé, R. (1992). *Crystallization of nucleic acids and proteins* 19-45 Oxford: Oxford University Press.

Luehr, C. A. and Schuster, S. M. (1985). *Arch. Biochem. Biophys.* **237**, 335-346.

Luzzati, V. (1952). *J. Appl. Crystallogr.* **5**, 802-810.

Matthews, B. W. (1968). *J. Mol. Biol.* **33**, 491-497.

Matthews, B. W., Remington, S. J., Grütter, M. G. and Anderson, W. F. (1981). *J. Mol. Biol.* **147**, 545-558.

Matthews, B. W. and Rossman, M. G. (1985). *Meth. Enzymol* **115**, 397-420. Orlando, FL: Academic Press.

Meister, A. (1974). *The Enzymes* **X**, 561-580 New York: Academic Press.

Moras, D. (1992). *Trends. Biochem. Sci.* **17**, 159-164.

Nakamura, M., Yamada, M., Hirota, Y., Sugimoto, K., Oka, A. and Takanami, M. (1981). *Nucleic Acids Res.* **9**, 4669-4676.

Neidhart, D. J., Fenyon, G. L., Gerlt, J. A. and Petsko, G. A. (1990). *Nature* **347**, 692-694.

Perona, J. J., Rould, M. A. and Steitz, T. A. (1993). *Biochemistry* **32**, 8758-8771.

Petsko, G. A., Kenyon, G. L., Gerlt, J. A., ringe, D. and Kozarich, W. (1993). *Trends. Biochem. Sci.* **18**, 372-376.

Poterszman, A., Delarue, M., Thierry, J.-C. and Moras, D. (1994). *J. Mol. Biol.* **244**, 158-167.

Ramachandran, G. N., Kolaskar, A. S., Ramakrishnan, C. and Sasisekharan, V. (1974). *Biochim. Biophys. Acta* **359**, 298-302.

Reitzer, L. J. and Magasanik, B. (1982). *J. Bacteriol.* **151**, 1299-1313.

Robertus, J. D., Alden, R. A., Birktoft, J. J., Kraut, J., Powers, J. C. and Wilcox, P. E. (1972). *Biochemistry* **11**, 2439-2449.

Ruff, M., Krishnaswamy, S., Boeglin, M., Poterszman, A., Mitshler, A., Podjarny, A., Rees, B., Thierry, J. C. and Moras, D. (1991). *Science* **252**, 1682-1689.

Sanger, F., Nicklen, S. and Coulson, A. R. (1977). *Proc. Natl. Acad. Sci. USA* **74**, 5463-5467.

Sato, M., Yamamoto, M., Imada, K., Katsube, Y., Tanaka, N. and Higashi, T. (1992). *J. Appl. Crystallogr.* **25**, 348-357.

Schimmel, P. (1987). *Annu. Rev. Biochem.* **56**, 125-158.

Scofield, M. A., Lewis, W. S. and Schuster, S. M. (1990). *J. Biol. Chem.* **265**, 12895-12902.

Sugiyama, A., Kato, H., Nishioka, T. and Oda, J. (1992). *Biosci. Biotech. Biochem* **56**, 376-379.

Wang, B.-C. (1985). *Meth. Enzymol.* **115**, 90-112. Orlando, FL: Academic Press.

Zalkin, H. (1993). *Adv. Enzymol. Relat. Areas Mol. Biol.* **66**, 203-309

List of Publications

Chapter 2

   Nakatsu, T., Kato, H. and Oda, J. (1996) *Acta Cryst.* **D52**, 604-606.

Chapter 3

   Nakatsu, T., Kato, H. and Oda, J. (1996) *Acta Cryst.* **A52**, Supplement C-114.
   Nakatsu, T., Kato, H. and Oda, J. (1997) *Photon Factory Activity Report* in press.

Chapter 4

   Nakatsu, T., Kato, H. and Oda, J. *manuscript in preparation.*